A novel framework for pixel-wise estimation of irrigation water use by integrating remote sensing and reanalysis data

Ling Zhang [a], Tao Che [a,*] , Kun Zhang [b], Donghai Zheng [c], Xin Li [c]

[a] Key Laboratory of Cryospheric Science and Frozen Soil Engineering, Heihe Remote Sensing Experimental Research Station, Northwest Institute of Eco-Environment and Resources, Chinese Academy of Sciences, Lanzhou 730000, China
[b] School of Geospatial Engineering and Science, Sun Yat-Sen University, Zhuhai, China
[c] National Tibetan Plateau Data Center, State Key Laboratory of Tibetan Plateau Earth System, Resource and Environment, Institute of Tibetan Plateau Research, Chinese Academy of Sciences, Beijing 100101, China

ARTICLE INFO

ABSTRACT

Accurate and spatially explicit estimates of irrigation water use (IWU) are essential for understanding the earth system dynamics in the Anthropocene. Recent advances in remote sensing have spurred growing interest in satellite-based IWU estimation. However, large-scale IWU estimates remain limited in both accuracy and spatial resolution due to inherent deficiencies in satellite observations and methodological constraints. Here, we present a novel framework for spatially explicit IWU estimation by integrating satellite-based soil moisture and evapotranspiration (ET) products with reanalysis data. Within this framework, we developed two alternative models: one based on root zone soil moisture (RSM) and the other on surface soil moisture (SSM), both grounded in soil water balance principles. The models estimate IWU by quantifying differences in soil moisture, ET, and drainage between natural and irrigated conditions. Both the RSM- and SSM-based models perform well in predicting prefecture-level IWU during the validation period, achieving coefficients of determination (R^2) between 0.72 and 0.90 and root mean square errors (RMSE) of 0.55–0.66 km³ /year, depending on the spatial scale of calibration (i. e., province, prefecture, or subregion). By combining our framework with different satellite products, we produce ensemble IWU estimates at 1 km resolution across China. The resulting dataset reveals a clear increasing trend in China's IWU from 2001 to 2020, primarily driven by the expansion of irrigated area, while its interannual variability is largely controlled by fluctuations in IWU per unit irrigated area. This dataset shows a significant advancement in both accuracy and spatial detail over existing datasets and will be useful for irrigation-related research and agricultural water management in China.

1. Introduction

Irrigation mitigates crop vulnerability to drought and heat stress, positioning as a key strategy for climate change adaptation (Zhu and Burney, 2022; Zhu et al., 2022; Driscoll et al., 2024). It plays a pivotal role in ensuring global food security (Zaveri and B. Lobell, 2019; Wang et al., 2021), contributing to 40 % of the world's food supply while occupying only 20 % of global croplands (UNESCO World Water Assessment Programme, 2019). Globally, irrigation is the largest consumer of freshwater, accounting for ~70 % of total water withdrawals and ~90 % of consumptive water use (Siebert and Döll, 2010; Qin et al., 2019). Over the past two decades, the area equipped for irrigation has expanded by 11 % globally, driving substantial gains in crop productivity (Mehta et al., 2024). However, the widespread use of irrigation has far-reaching impacts on the earth system, including alterations to the surface energy balance, hydrological processes, and biogeochemical cycles, while simultaneously placing increasing pressure on freshwater resources (McDermid et al., 2023; Yang et al., 2023; Driscoll et al., 2024; Qin et al., 2024). Given irrigation's central role in both food production and Earth system dynamics, there is a pressing need to understand the spatiotemporal patterns of irrigation water use (IWU).

IWU is a broad term that may refer to total irrigation water withdrawals (from rivers, reservoirs, or aquifers), field-level irrigation water applications, or consumptive irrigation water use through evapotranspiration. Numerous efforts have been made to estimate IWU, which can

be broadly categorized into three main approaches: physical modeling, machine learning, and remote sensing. Physical modeling estimates IWU using process-based models such as hydrological, land surface, or crop models (Döll and Siebert, 2002; Jägermeyr et al., 2015; Huang et al., 2020; Yin et al., 2020b; Zhou et al., 2020b; Han et al., 2023). While these models can produce IWU estimates at high spatial and temporal resolution, they often suffer considerable uncertainty arising from over-simplified or inconsistent representations of irrigation processes and the limited availability of direct IWU observations for model calibration (Hu et al., 2016; Chen et al., 2019; Foster et al., 2019; Zaussinger et al., 2019; Koch et al., 2020). In contrast, machine learning (ML) techniques do not require predefined physical assumptions and are particularly effective at capturing complex interactions and nonlinear relationships between IWU and its controlling factors (Wongso et al., 2020; Bhattarai et al., 2021; Zhang et al., 2022c; Lu et al., 2023; Alkon and Wang, 2024). This makes ML a promising alternative to physical models for IWU estimation (Majumdar et al., 2020, 2022; Filippelli et al., 2022; Bo et al., 2024; Ott et al., 2024). However, ML approaches are often criticized for their "black box" nature (Ma et al., 2023; Jung et al., 2024), and their predictive performance depends greatly on the quantity and quality of the training data. Given that IWU observations are unavailable in many regions due to technical, economic, or political constraints (Foster et al., 2020), the application of ML methods for IWU estimation remains challenging.

Remote sensing techniques have advanced considerably over the past few decades, making it increasingly feasible to estimate IWU from space (Zhang et al., 2022a; Dari et al., 2023a). Leveraging satellite observations and hydrological principles, remote sensing-based IWU estimation has emerged as a rapidly growing area of research across both the remote sensing and hydrology communities (Foster et al., 2020; Brookfield et al., 2023). Existing remote sensing approaches to IWU estimation can be classified into two main categories: soil moisture-based and evapotranspiration (ET)-based methods (Dari et al., 2023b; Kragh et al., 2023a).

Soil moisture-based approach approaches estimate IWU by detecting irrigation-induced changes in soil moisture (Zaussinger et al., 2019; Zohaib and Choi, 2020) or by applying soil water balance frameworks such as the Soil Moisture to Rain (SM2RAIN) algorithm that conceptualize irrigation as an equivalent to rainfall (Brocca et al., 2013, 2018). These methods have been successfully applied across a wide range of spatial scales, from field to global levels (Filippucci et al., 2020; Dari et al., 2022, 2023b; Zhang et al., 2022a). However, soil moisture-based approaches generally require high-temporal-resolution soil moisture data and often produce IWU estimates at coarse spatial resolutions, with a tendency to underestimate actual IWU (Zhang and Long, 2021). These limitations primarily arise from the inherent shortcomings of satellite soil moisture products (e.g., low spatial resolution, data gaps) and the shortcomings of estimation algorithms. Another strand of soil moisture-based methods estimates irrigation by assimilating satellite-derived soil moisture into land surface models equipped with irrigation modules (Abolafia Rosenzweig et al., 2019; Jalilvand et al., 2023; Busschaert et al., 2024; Laluet et al., 2024). While effective at local scales, the applicability of these data assimilation approaches to larger regions remains limited, as they typically require extensive calibration against in situ measurements and are sensitive to regional heterogeneity in irrigation practices, making them both time-consuming and computationally intensive (Majumdar et al., 2020; Olivera-Guerra et al., 2023).

In contrast, ET-based approaches estimate irrigation by analyzing residuals between satellite-derived ET and baseline values obtained either from hydrological or land surface models under rainfed conditions, or from hydrologically similar neighboring pixels (Cheema et al., 2014; van Eekelen et al., 2015; Peña-Arancibia et al., 2016; Chen et al., 2019; Koch et al., 2020; Yin et al., 2020a; Brombacher et al., 2022; Boser et al., 2024). Compared with soil moisture-based methods, ET-based approaches offer notable advantages, particularly in enabling IWU

estimation at finer spatial resolutions—ranging from 30 m to 1 km (Koch et al., 2020; Boser et al., 2024). Furthermore, ET is directly linked to plant transpiration in response to irrigation, whereas soil moisture provides only an indirect estimate (Kragh et al., 2023a, 2023b). However, ET-based methods typically neglect irrigation-induced changes in soil moisture and subsurface drainage, thereby quantifying only the consumptive component of water use rather than the total irrigation water applied or withdrawn (Laluet et al., 2024). This limitation complicates validation efforts, as consumptive use cannot be directly measured (Zhang et al., 2022c). In practice, consumptive water use is often converted to actual IWU using irrigation efficiency, yet this parameter is difficult to determine accurately at fine spatial scales, introducing substantial uncertainty (Puy and Lankford, 2022). An alternative strategy is to calibrate hydrological or soil water balance models against satellite-derived ET and estimate IWU inversely through embedded irrigation modules. However, this inverse modeling approach is computationally expensive, especially when applied at national or global scales; and meanwhile, the results are highly sensitive to model assumptions on irrigation process.

Despite considerable progress in satellite-based IWU estimation, several limitations remain. First, although many studies have demonstrated promising performance at local or basin scales, few have tested the transferability of their models across broader spatial domains, resulting in a scarcity of publicly available, remotely sensing-derived IWU datasets (Dari et al., 2023b). Existing global-scale IWU products are typically characterized by coarse spatial resolution (e.g., 0.25°) and limited accuracy (Chen et al., 2019; Zhang et al., 2022a), which restrict their applicability for regional or local-scale analyses. Second, neither soil moisture nor ET al.one can fully capture irrigation inputs. Recent studies have highlighted the advantages of jointly using soil moisture and ET for IWU estimation (Zhang and Long, 2021; Kragh et al., 2023a), yet most existing approaches exclusively on one of these variables (Supplementary Table S1). Third, few studies have compared their IWU estimation approaches against ML models. This lack of cross-method comparison hinders a comprehensive understanding of the relative strengths and weaknesses of existing approaches. Finally, satellite-derived SM and ET products are inherently uncertain. While integrating multiple remote sensing sources can improve IWU accuracy (Zhang et al., 2022a; Bo et al., 2024), the sensitivity of IWU estimates to product selection and data fusion strategies remains insufficiently explored.

To address these gaps, this study presents a novel framework for spatially explicit estimation of IWU by integrating satellite-based soil moisture and ET products with reanalysis data. This framework comprises two alternative IWU estimation models: one based on root zone soil moisture (RSM) and the other on surface soil moisture (SSM), both grounded in soil water balance between natural and irrigated conditions. Building on this framework and ensemble techniques, including the summed square error and Bayesian Three-Cornered Hat methods, we generate 1 km IWU estimates across China for the period 2001–2020. The specific objectives of this study are to: (1) evaluate the performance of the RSM- and SSM-based models; (2) compare their performance with the widely used Random Forest (RF) algorithm; (3) assess the influence of using and integrating different remote sensing datasets; and (4) validate the ensemble IWU dataset against independent reports and compare it with existing products.

2. Material and methods

As shown in Fig. 1, the workflow of this study consists of five major steps. Following data acquisition and preprocessing, we calibrated and evaluated two alternative IWU estimation models derived from root zone and surface soil moisture balances, respectively. Next, we compared their performance with that of the RF algorithm across different temporal periods and spatial scales of model training and calibration. In the third step, we examined the sensitivity of model
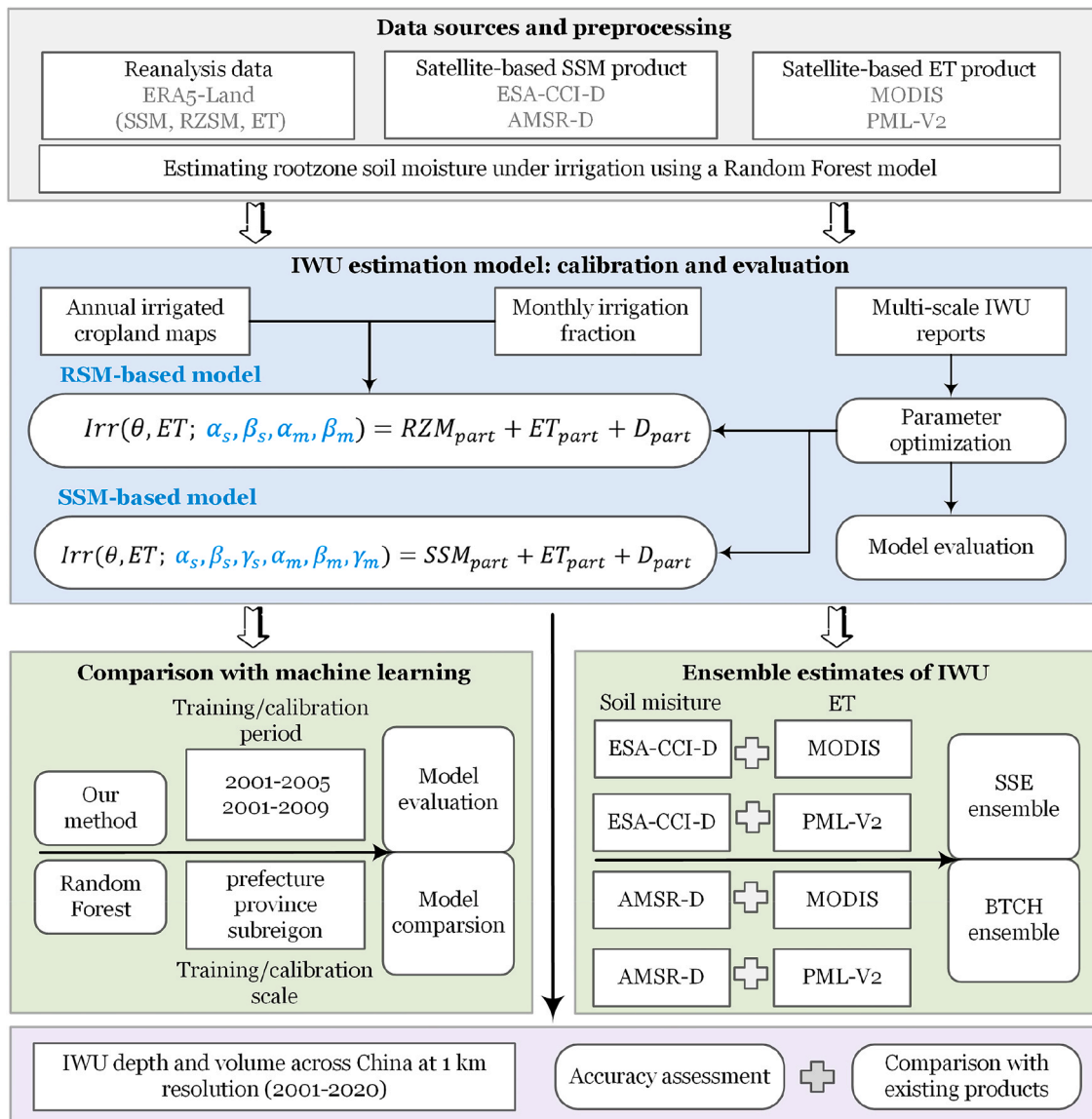
Fig. 1. Workflow of the study.

performance to the use and integration of multiple satellite-based ET and SSM products. Two ensemble integration methods, i.e., the summed square error approach and the Bayesian Three-Cornered Hat method, were tested and compared. Finally, we generated IWU estimates across China using the proposed models in conjunction with the best-performing ensemble technique. The resulting dataset was validated against independent IWU reports and further evaluated through comparisons with existing IWU products.

2.1. Study area

This study focuses on mainland China, a region characterized by extensive croplands, diverse topography, and pronounced climatic variability (Fig. 2). As one of the world's major agricultural countries, China had approximately 160 million hectares (Mha) of cropland in 2020 (Zhang et al., 2024a). Irrigated and rainfed croplands account for approximately 60 % and 40 % of China's total cropland area, respectively. Among all subregions, South China contains the largest share of the national total irrigated cropland (26 %), followed by Central South, North, Northwest, Southwest, and Northeast China. In contrast, rainfed croplands are mainly concentrated in the southwestern, central, and

northeastern parts of the country. Over the past two decades, China's irrigated area has expanded by about 18 Mha (or 25 %), with the majority of this expansion (~60 %) occurring in water-scarce regions facing severe to extreme water stress (Zhang et al., 2024b). This rapid expansion has intensified concerns about water scarcity in China, highlighting the urgent need for spatially explicit estimates of IWU to support sustainable agricultural water management.

2.2. Data sources and preprocessing

2.2.1. Reanalysis data

In this study, we utilized monthly soil moisture and ET data from the land component of the fifth generation of the European ReAnalysis (ERA5-land) (Muñoz-Sabater et al., 2021). ERA5-land provides a consistent view of land variables over several decades at a higher resolution of 0.01°, compared to the coarser resolution of 0.25° in ERA5. The mean volumetric soil water content is reported for four soil layers corresponding to depths of 0–7, 7–28, 28–100, and 100–289 cm. Surface soil moisture (SSM) was represented by the soil water content in the first layer (0–7 cm). Root-zone soil moisture (RSM) was estimated by summing the soil water content from the first three layers, weighted at 0.40,
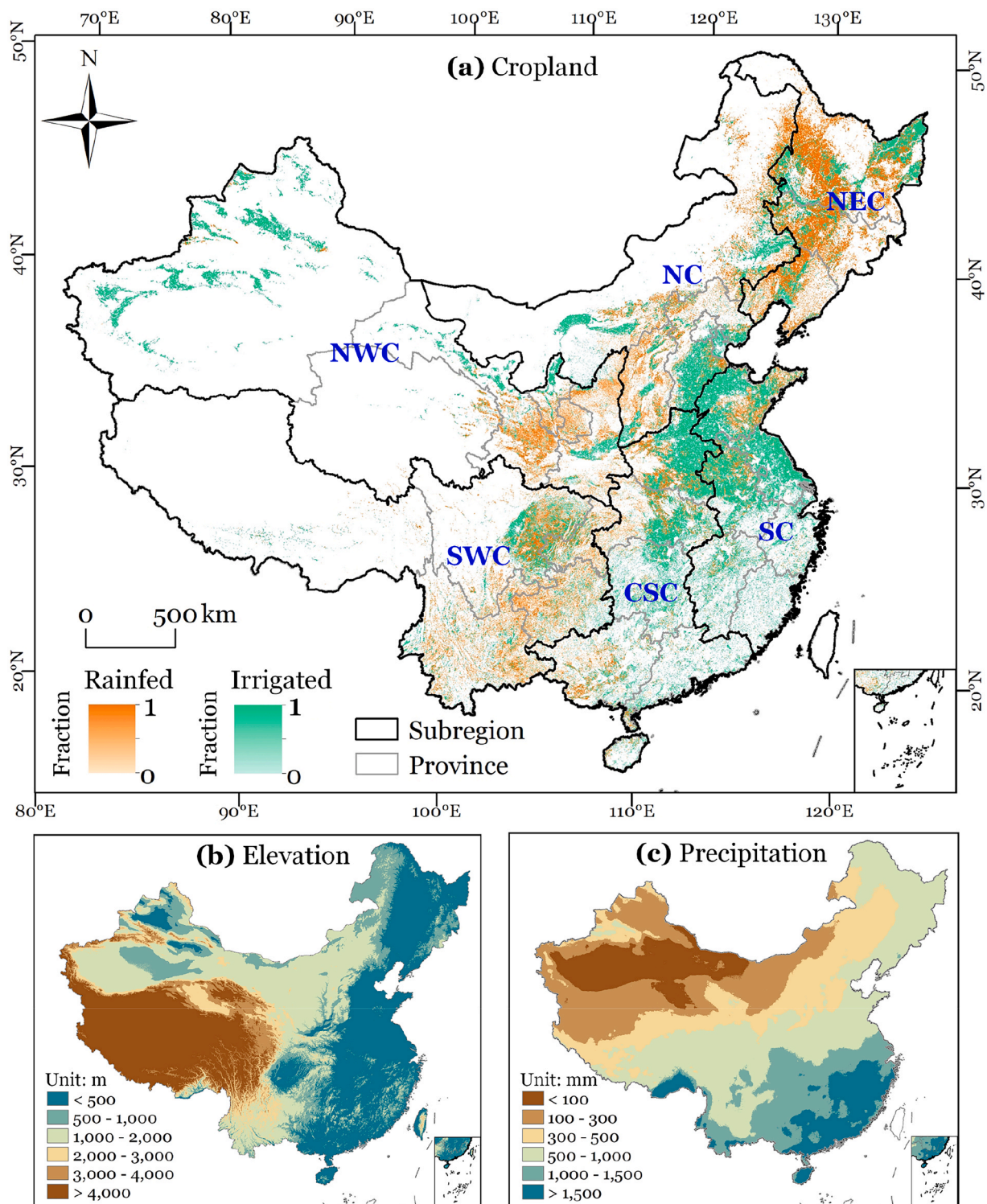
Fig. 2. Overview of the study area. Panel (a) shows the distribution of irrigated and rainfed croplands cross mainland China in 2020. Panel (b) and (c) present the spatial patterns of elevation and multi-year (1991–2020) average precipitation, respectively. NEC, NC, NWC, SWC, SC and CSC represent Northeast China, North China, Northwest China, Southwest China, South China, and Central South China, respectively.

0.35, and 0.25, respectively, following the study of Zhang and Long (2021). All SSM, RSM, and ET data were resampled to 1 km resolution using nearest-neighbor interpolation to preserve the original data characteristics while maintaining computational efficiency.

2.2.2. Remote sensing data

This study utilized two satellite-based ET products and two satellite-

derived SSM products. The Moderate Resolution Imaging Spectroradiometer (MODIS) ET product is calculated using the Penman-Monteith equation (Monteith, 1965), which incorporates daily meteorological reanalysis data along with MODIS-derived vegetation dynamics, albedo, and land cover (Mu et al., 2011). Specifically, we employed the MOD16A2GF product, an enhanced version of MOD16, providing 8-day ET estimates at 500 m resolution. The PML-V2 ET product is developed

using the Penman-Monteith-Leuning model Version 2 and provides daily ET estimates at 500 m resolution for the period 2000–2020 (Zhang et al., 2019; He et al., 2022).

The AMSR-D product provides daily surface soil moisture at 1 km resolution, offering improved coverage under all-weather conditions across China (Song et al., 2022). The suffix "D" indicates that this product is a downscaled version of the original 36 km AMSR-E/AMSR-2 SSM data. The product shows good agreement with in situ soil moisture measurements from over 2000 meteorological stations, with unbiased root mean square difference (RMSD) values ranging from 0.052 to 0.059 m^3/m^3 (Song et al., 2022). The ERA-CCI-D product is a 21-year dataset (2000–2020) of gap-free global daily surface soil moisture at 1 km resolution (Zheng et al., 2023). The suffix "D" denotes that the product is a downscaled version of the original ERA-CCI SSM dataset, generated using a RF algorithm that incorporates gap-filled ERA-CCI data, in situ observations, and optical remote sensing data. The high-resolution product exhibits good accuracy when cross-validated against in-situ soil moisture observations from the International Soil Moisture Network, achieving a correlation coefficient of 0.89 (Zheng et al., 2023).

2.2.3. Root zone soil moisture under irrigation

Satellite-derived soil moisture products provide spatially explicit estimates of near-surface soil moisture under actual (irrigated) conditions; however, they primarily reflect the water content in the top few centimeters of the soil profile (Ford et al., 2014). In this study, we estimated monthly RSM under irrigation from satellite-based SSM and ET data. Following the previous study (Zhang and Long, 2021), we first constructed a RF model (Eq. 1) to learn the relationships between RSM and predictors (i.e., precipitation, ET, SSM, and ET/PET) under rainfed conditions (Supplementary Figure S1). The model was then applied to estimate RSM under irrigation using satellite-based SSM and ET data, as shown in Eq. (2).

$$\theta_m^{rz} = f\left(\frac{ET_m}{PET}, Prec, ET_m, \theta_m^{sf}\right) + \varepsilon \tag{1}$$

$$\theta_s^{rz} = f\left(\frac{ET_s}{PET}, Prec, ET_s, \theta_s^{sf}\right) \tag{2}$$

where θ_m^{rz} and θ_s^{rz} represent the ERA5-land derived RSM and the estimated RSM under irrigation, respectively; ET_m and ET_s indicate modeled and satellite-based ET, respectively; θ_m^{sf} and θ_s^{sf} indicate modeled and satellite-based surface soil moisture, respectively; $Prec$ and PET denote precipitation and potential evapotranspiration, respectively; f is the Random Forest model, and ε signifies model error. In this study, precipitation data at 1 km resolution were sourced from ChinaMet (Zhang et al., 2021; Hu et al., 2024), which integrates gauge observations, multisource satellite products, and reanalysis data. PET was estimated using the Hargreaves method (Hargreaves, 1994), based on latitude, day of the year, and temperature data.

2.2.4. Irrigation data

This study used several irrigation-related data including IWU reports, irrigated cropland maps, and monthly irrigation fractions. The IWU reports, covering the period from 2000 to 2020 for 357 prefectures, were sourced from the Water Resources Departments of 31 provinces of China (Zhang et al., 2023) and the China Economic and Social Big Data Research Platform (https://data.cnki.net/). Here, IWU refers to the total volume of water withdrawn from rivers, reservoirs, and aquifers for crop irrigation, accounting for transportation and application losses. Annual maps of China's irrigated cropland (i.e., CIrrMap250) were developed in our previous study by integrating multiple remote sensing datasets, reported statistics, surveys, and irrigation suitability analyses (Zhang et al., 2024b). These maps reflect the maximum irrigated area for each year, with pixels classified as irrigated if they were irrigated at any time during that year. Hence, we additionally derived the monthly irrigation

fractions for each prefecture of China from our global satellite-based IWU product (Zhang et al., 2022a), calculated as the ratio of the irrigated area in a given month to the maximum irrigated area for that year in each prefecture. We also obtained monthly irrigation fractions for Northeast, Southeast, and West China from the Food and Agriculture Organization of the United Nations (FAO, 2006).

2.3. Theoretical foundation for the IWU estimation framework

2.3.1. Rootzone soil moisture-based model

Our IWU estimation framework assumes that satellite-based soil moisture and ET retrievals capture irrigation signals, while reanalysis model simulations do not, in line with previous studies (Wei et al., 2013; Romaguera et al., 2014a, 2014b; Zaussinger et al., 2019; Zohaib and Choi, 2020; Zhang and Long, 2021). The soil water balance for the root zone under irrigated conditions (Fig. 3a) is described by the following equation:

$$z^{rz} * \frac{d\theta_s^{rz}}{dt} = Prec(t) + Irr(t) - ET_s(t) - Dp_s(t) - LF_s(t) - R \tag{3}$$

where z^{rz} is root zone depth (mm); θ^{rz} is root zone soil moisture (m^3/m^3); $Prec$ is precipitation (mm); Irr is irrigation (mm), ET is evapotranspiration; Dp is deep percolation (mm); LF is lateral flow (mm); R is surface runoff (mm); and t represents the time step (month). The subscript s indicates variables derived from satellite observations. The combined effect of deep percolation and lateral flow is treated as drainage (D), which is estimated from relative soil moisture (i.e., degree of saturation) using a power-law function (Brocca et al., 2013; Li et al., 2023):

$$D_s(t) = \alpha_s * \left(\frac{\theta_s^{rz}}{\varphi}\right)^{\beta_s} \tag{4}$$

where α_s and β_s are the empirical drainage parameters; φ is soil porosity of the root zone, derived from the China dataset of soil hydraulic parameters (Shangguan et al., 2013). By substituting Eq. (4) into Eq. (3) and assuming negligible surface runoff in irrigated croplands, the soil water balance simplifies to:

$$z^{rz} * \frac{d\theta_s^{rz}}{dt} = Prec(t) + Irr(t) - ET_s(t) - D_s(t) \tag{5}$$

As shown in Fig. 3b, the soil water balance for the root zone under natural (i.e., rainfed) conditions is described using soil moisture and ET estimates from ERA5-Land under the assumption that irrigation is an unmodeled hydrological process in reanalysis models (Zaussinger et al., 2019; Muñoz-Sabater et al., 2021; Zhang and Long, 2021):

$$z^{rz} * \frac{d\theta_m^{rz}}{dt} = Prec(t) - ET_m(t) - D_m(t) \tag{6}$$

where θ_m^{rz} and ET_m are the ERA5-Land modeled root zone soil moisture and evapotranspiration, respectively; and D_m is the drainage estimated from θ_m^{rz}, similar to Eq. (4). Subtracting Eq. (6) from Eq. (5) yields the RSM-based irrigation estimate model:

$$Irr(\theta, ET; \alpha_s, \beta_s, \alpha_m, \beta_m) = RSM_{part} + ET_{part} + D_{part} \tag{7}$$

$$RSM_{part} = z^{rz} * \left(\Delta\theta_s^{rz} - \Delta\theta_m^{rz}\right) \tag{8}$$

$$ET_{part} = (ET_s - ET_m) - bias \tag{9}$$

$$D_{part} = \left(\alpha_s * \left(\frac{\theta_s^{rz}}{\varphi}\right)^{\beta_s} - \alpha_m * \left(\frac{\theta_m^{rz}}{\varphi}\right)^{\beta_m}\right) \tag{10}$$

where θ and ET are the model inputs, while $\alpha_s, \beta_s, \alpha_m, \beta_m$ are the unknown parameters to be calibrated. The $bias$ represents the spatially average difference between satellite-based and modeled ET over rain-
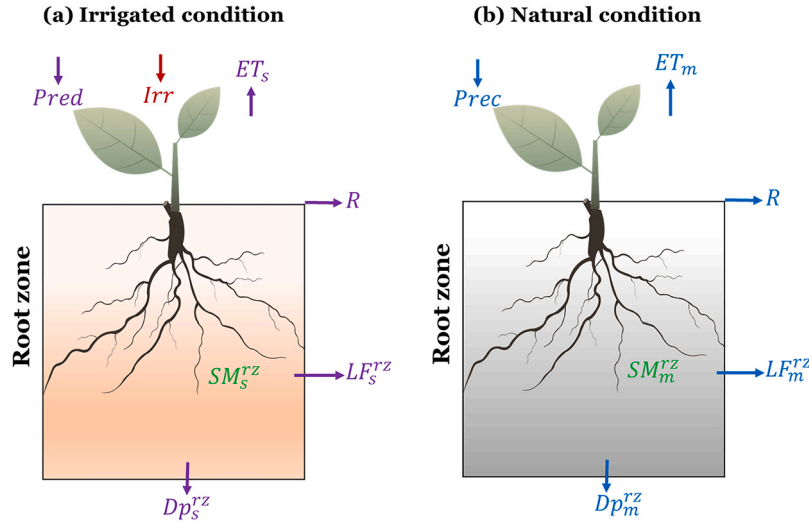
(a) Irrigated condition   (b) Natural condition

Fig. 3. Soil water blance for the root zone under irrigated (a) and natural (b) conditions. The definitions of the variables are provided in Eqs. (3) and (6).

fed cropland pixels, identified using our cropland and irrigated cropland maps (Zhang et al., 2024a, 2024b). In our case, the biases are approximately −9 and −11 mm/month for the MODIS and PML-V2 products, respectively, exhibiting noticeable month-to-month variations (Supplementary Figure S2).

2.3.2. Surface soil moisture-based model

The soil water balance for the surface layer of the root zone under irrigated conditions (Fig. 4a) is described using satellite-derived soil moisture and ET, as follows:

$$z^{sf} * \frac{d\theta_s^{sf}}{dt} = Prec(t) + Irr(t) - E_s^{sf} - D_s^{sf}(t) \tag{11}$$

where z^{sf} is depth of the surface layer within the root zone (mm); θ_s^{sf} is soil moisture in the surface layer (m³/m³); $D_s^{sf}(t)$ is drainage from the surface layer, including both percolation and lateral flow, estimated using a power-law function as in Eq. (4); and E_s^{sf} is evaporation from the surface layer of the root zone, calculated as $ET_s - T_s^{sub}$, where ET_s is total evapotranspiration, and T_s^{sub} is transpiration from the subsurface layer, estimated as follows:

$$ET_s^{sub} = \gamma_s * ET_s \tag{12}$$

where γ_s is fraction of total evapotranspiration attributable to subsurface transpiration. Under natural conditions (Fig. 4b), the soil water balance for the surface layer is given by:

$$z^{sf} * \frac{d\theta_m^{sf}}{dt} = Prec(t) - E_m^{sf} - D_m^{sf}(t) \tag{13}$$

where θ_m^{sf}, D_m^{sf}, and E_m^{sf} are the ERA5-Land modeled surface soil moisture, drainage, and evaporation, respectively. Similarly, E_m^{sf} is estimated as the difference between ET_m and T_m^{sub}, where ET_m is the modeled total evapotranspiration and $T_m^{sub} = \gamma_m * ET_m$ is the modeled transpiration. Subtracting Eq. (13) from Eq. (11) yields the SSM-based irrigation estimate model:

$$Irr(\theta, ET; \alpha_s, \beta_s, \gamma_s, \alpha_m, \beta_m, \gamma_m) = SSM_{part} + ET_{part} + D_{part} \tag{14}$$

$$SSM_{part} = z_{sf} * \left(\Delta\theta_s^{sf} - \Delta\theta_m^{sf} \right) \tag{15}$$

$$ET_{part} = (ET_s - ET_m) - bias \tag{16}$$

$$D_{part} = \left(\alpha_s * \left(\frac{\theta_s^{sf}}{\varphi} \right)^{\beta_s} - \gamma_s ET_s \right) - \left(\alpha_m * \left(\frac{\theta_m^{sf}}{\varphi} \right)^{\beta_m} - \gamma_m ET_m \right) \tag{17}$$

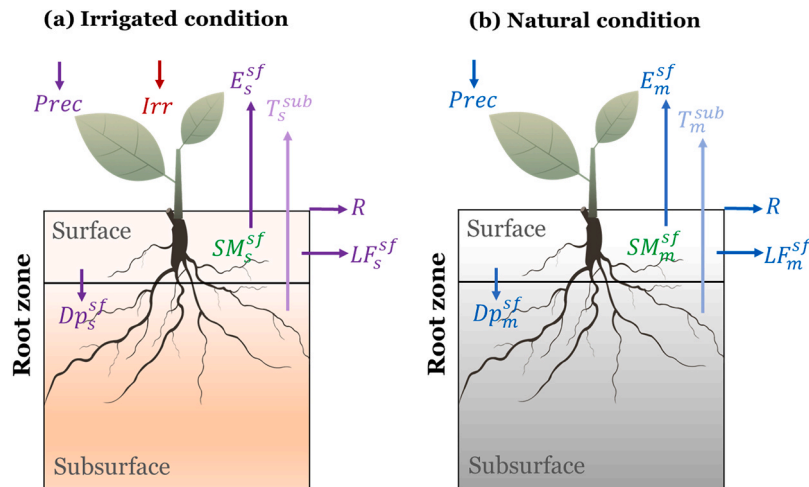## (a) Irrigated condition   (b) Natural condition

Fig. 4. Soil water blance for the surface layer of the root zone under irrigated (a) and natural (b) conditions. The definitions of the variables are provided in Eqs. (11) and (13).

where θ and ET are the model inputs; $\alpha_s, \beta_s, \gamma_s, \alpha_m, \beta_m, \gamma_m$ are the unknown parameters to be calibrated; and *bias* is the spatially averaged difference between modeled and satellite-derived evapotranspiration over rainfed pixels. To account for systematic differences between satellite and modeled soil moisture, ERA5-land SSM were rescaled by subtracting its mean and adding the mean of the satellite-based SSM (Kragh et al., 2023a). In this study, the parameters used to rescale ERA5-Land SSM have median values of -0.075 and -0.080 m³/m³ across cropland grids in China for the ESA-CCI-D and AMSR-D products, respectively (Supplementary Figure S3).

2.4. Model calibrating and validation

The parameters of the RSM- and SSM-based models were calibrated by minimizing the error between the estimated and reported annual irrigation depth (i.e., IWU per unit irrigated area):

$$SSE = \sum_j^n \left(EIrr_{j,t}^d - RIrr_{j,t}^d \right)^2 \tag{18}$$

where *SSE* is the objective function; $EIrr_j^d$ and $RIrr_j^d$ denote the estimated and reported irrigation depth, respectively, for administrative unit j in year t; and n is the total number of administrate units used for calibration. The estimated and reported annual irrigation depth are calculated as follows:

$$EIrr_{j,t}^d = \frac{1}{N_j}\sum_{i=1}^{N_j}\sum_{m=1}^{12} Irr_{j,t}^{i,m} \tag{19}$$

$$RIrr_{j,t}^d = IWU_{j,t}^v / IA_{j,t}^{act} \tag{20}$$

where $Irr_{j,t}^{i,m}$ is the estimated irrigation depth per unit irrigated area for grid i and month m (with a lower bound of 0); N_j denotes the number of irrigated cropland grids in administrative unit j; $IWU_{j,t}^v$ is the the reported volumetric IWU (km³/year), and $IA_{j,t}^{act}$ represents the actual irrigated area in year t, calculated as:

$$IA_{j,t}^{act} = \frac{1}{12}\sum_m^{12}(IA_{j,t}^{max} \times IF_{j,t,m}) \tag{21}$$

where IA_j^{max} is the maximum irrigated area for administrate unit j in year t, derived from the CIrrMap250 dataset (Zhang et al., 2024b); and $IF_{j,t,m}$ the monthly fraction of area actually irrigated, estimated from our global satellite-based IWU product (Zhang et al., 2022a).

Our monthly irrigation fraction estimates show reasonable agreement with those reported by FAO (2006) and the recently developed MIRCA-OS product (Kebede et al., 2025), with correlation coefficients of 0.58 and 0.64, respectively, across Northeast, Southeast, and Western China (Supplementary Figure S4). Model parameters were calibrated separately using IWU reports aggregated at three spatial scales, i.e., subregion, province, and prefecture (Supplementary Figure S5). This design was intended to evaluate how the spatial resolution of reference data influences model performance and to assess the model's robustness under varying data availability conditions. Model optimization was performed using the GlobalSearch solver in MATLAB and repeated ten times to minimize the influence of local minima and enhance parameter stability. The calibrated models were subsequently used to predict monthly irrigation volumes at the grid level, and annual IWU for each administrative unit was obtained by aggregating the monthly values:

$$IWU_{j,t}^{act} = \sum_{i=1}^{N_j}\sum_{m=1}^{12} Irr_{j,t}^{i,m} \times IA_{j,t}^{max} \times IF_{j,t,m} \tag{22}$$

The model predictions were evaluated using prefecture-level IWU reports during the validation period 2010–2020 using the performance metrics including the coefficient of determination (R²), root mean square error (RMSE), and bias.

2.5. Comparison with machine learning

We benchmarked our IWU estimation models against the RF algorithm (Breiman, 2001), a widely adopted ensemble machine learning method in hydrology and remote sensing. The RF model was trained using socioeconomic, climatic, auxiliary, and remote sensing and reanalysis-based predictors (Supplementary Table S2). Socioeconomic predictors included population and gross domestic product; climatic predictors comprised precipitation and PET; and auxiliary predictors included irrigation efficiency, elevation, slope, soil depth, soil porosity, and geographic coordinates (longitude and latitude). In addition, we incorporated several remote sensing and reanalysis-based predictors into the RF model, including ET, SSM, RSM, normalized difference vegetation index, and two components form our SSM-based model (i.e., SSM_{part} and ET_{part}).

We trained six RF models using IWU reports aggregated at different administrative levels (subregion, province, and prefecture) over two distinct periods (2001–2005 and 2001–2009). These variations in administrative scale and data volume enable us to assess the model's sensitivity to reference data availability and its robustness under limited-data conditions. The hyperparameters of the RF models, including the number of trees and the minimum number of observations per leaf, were optimized via a grid-search procedure. All prefecture-level IWU data for 2010–2020 were used for model validation. As these data were not included in the training phase, they provide an independent dataset for evaluating model performance. The RF models were then compared with our IWU estimation models under equivalent data availability scenarios, enabling a robust assessment of relative model effectiveness.

2.6. Ensemble estimates of IWU

We utilized two satellite-based ET products (MODIS and PML-V2) and two SSM products (ERA-CCI-D and AMSR-D), resulting in four unique SSM-ET combinations. The performance of our IWU estimation models was evaluated for each product combination. The resulting IWU estimates were then combined using a weighted ensemble approach:

$$IWU_{ens} = \sum_{k=1}^N w_k \times IWU_k \tag{23}$$

where N is the number of ensemble members ($N = 4$); and w_k is the weight assigned to the k-th member. Two weighting schemes were tested: the summed squared error (SSE) method and the Bayesian Three-Cornered Hat (BTCH) approach (Xu et al., 2019; He et al., 2020):

$$w_k^{SSE} = \frac{SSE_k^{-1}}{\sum_{k=1}^N SSE_k^{-1}} \tag{24}$$

$$w_k^{BTCH} = \frac{\prod_{i=1,i\neq k}^N \sigma_i^2}{\sum_{k=1}^N \left(\prod_{i=1,i\neq k}^N \sigma_i^2\right)} \tag{25}$$

where SSE_k denotes the summed squared error of the k-th IWU estimate relative to reported values, and σ_i is the error covariance of ensemble member i, estimated using the Three-Cornered Hat (TCH) method. The ensemble performance was evaluated for the validation period 2010–2020 and benchmarked against the individual ensemble members.

Based on the comparative performance of the IWU estimation models (RSM vs. SSM-based) and the ensemble techniques (SSE vs. BTCH), we selected the optimal configuration to generate pixel-wise estimation of IWU across China from 2001 to 2020. The resulting IWU dataset was compared against three existing products: IWU-Huang (Huang et al., 2018), IWU-Cheng (Chen et al., 2019), and IWU-Zhang (Zhang et al.,

2022a). The accuracy of our IWU estimates and the existing datasets was evaluated using independent IWU reports collected from local water resource authorities, covering 10 major basins, 21 sub-basins, and 124 sub-prefectures (counties) across China (Supplementary Figure S6).

3. Results

3.1. Performance of the IWU estimation models

As illustrated in Fig. 5, both the RSM- and SSM-based IWU estimation models perform well during the validation period (2010–2020), achieving R^2 values of 0.84 and 0.90, respectively. However, both models exhibit a systematic overestimation of IWU, with positive biases of 0.10 and 0.24 km³ /year, respectively. This bias likely arises from irrigation efficiency effects. Because our model was calibrated against census-based IWU data, which refers to the total volume of irrigation water withdrawals including conveyance losses, a key component of irrigation efficiency (i.e., conveyance efficiency) is implicitly embedded within the calibrated parameters. Consequently, parameters calibrated for earlier years (2001–2005) would overpredict IWU in later years (2010–2020), when irrigation efficiency had substantially improved (Zhang et al., 2023). As expected, model performance decreases when the calibration scale shifts from prefecture to provincial and subregional levels, highlighting the sensitivity of model accuracy to calibration data resolution. Nevertheless, both models maintain satisfactory performance at coarser calibration scales, with R^2 values ranging from 0.72 to 0.80 and RMSE values between 0.55 and 0.65 km³ /year. The SSM-based model achieves higher R^2 values than the RSM-based model, possibly due to the RSM estimation errors under irrigated conditions. In contrast, the RSM-based model shows lower bias and RMSE, likely due to its simpler parameterization, which facilitates convergence toward global optimal solutions during calibration.

3.2. Comparison with the Random Forest model

Fig. 6 compares the performance of our models with that of the RF algorithm. Both the RSM- and SSM-based models consistently outperform RF, exhibiting higher R^2 and lower RMSE. Specifically, our models improve R^2 by 3–11 % and reduce RMSE by 3–15 % relative to RF when calibrated or trained with prefecture-level IWU reports. Extending the calibration or training period further enhances the accuracy of all models. However, as the spatial scale of the reference data increases from prefectural to subregional levels, the performance of all approaches declines, with the deterioration being more pronounced for RF. Consequently, the relative performance advantage of our models becomes greater under coarse-scale data conditions. These findings demonstrate that our models are not only more accurate but also more robust than the RF algorithm across varying data availability scenarios.

3.3. Influence of using and integrating different remote sensing data

As shown in Fig. 7, the choice of remote sensing products (i.e., SSM and ET) exerts a substantial influence on the accuracy of both the RSM- and SSM-based models, with differences in R^2 reaching up to 0.15 and differences in RMSE up to 0.4 km³ /year. Among all product combinations, the ESA-CCI-D SSM and MODIS ET lead to the best model performance. These results underscore the critical role of data source selection in enhancing the reliability of IWU estimation. Regardless of the data used, the R^2 values for both models consistently decrease as the model calibration scales increase from prefectural to subregional levels. In contrast, RMSE does not show a clear dependence on model calibration scale. In terms of R^2, the SSM-based model consistently outperforms the RSM-based model; however, regarding RMSE, its relative accuracy varies depending on the specific product combination.

As shown in Fig. 8, both the SSE and BTCH ensemble techniques enhance model performance, increasing R^2 by up to 3 % and 13 % and
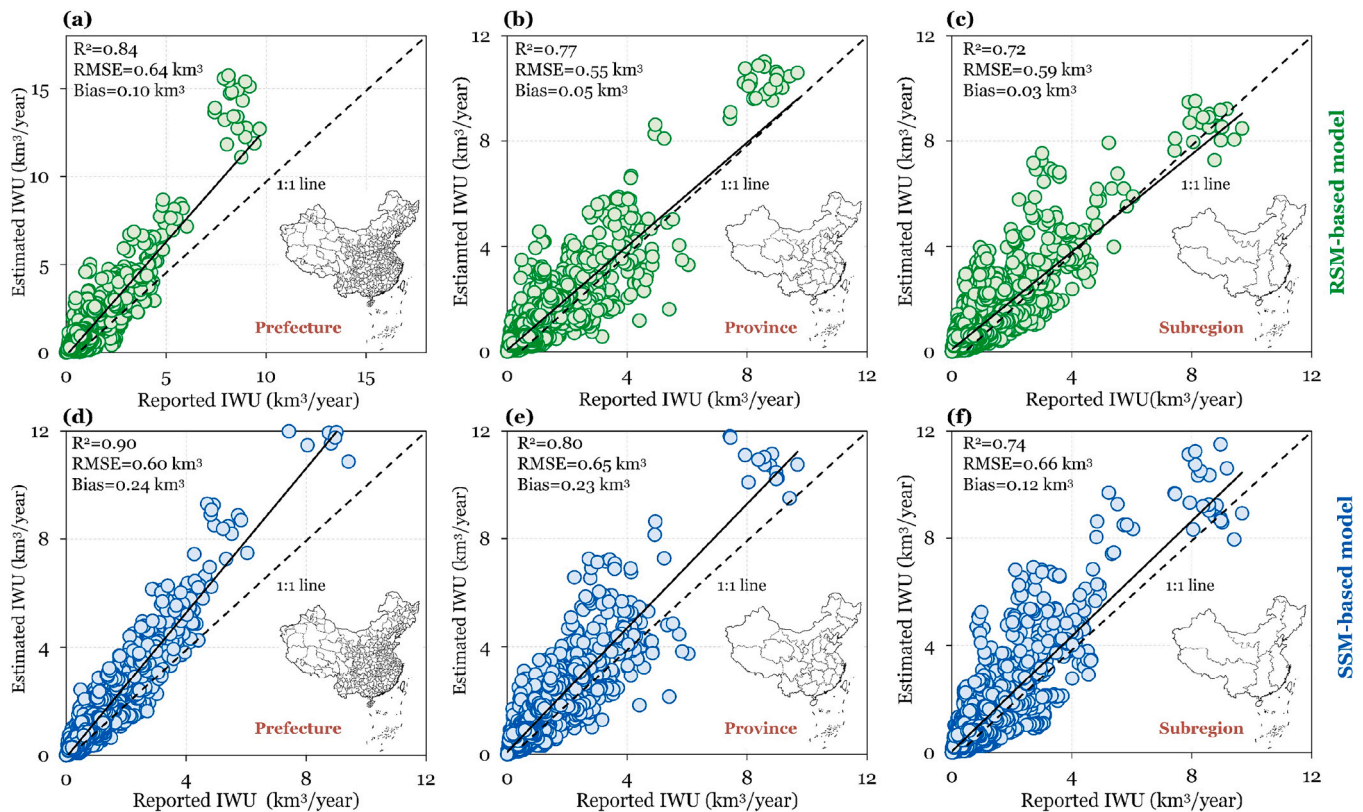

Fig. 5. Model accuracy in estimating prefecture-level IWU during the validation period (2010–2020). The top and bottom panels correspond to the RSM- and SSM-based models, respectively. From left to right, results are shown for models calibrated at the prefectural, provincial, and subregional levels for the period 2001–2005.
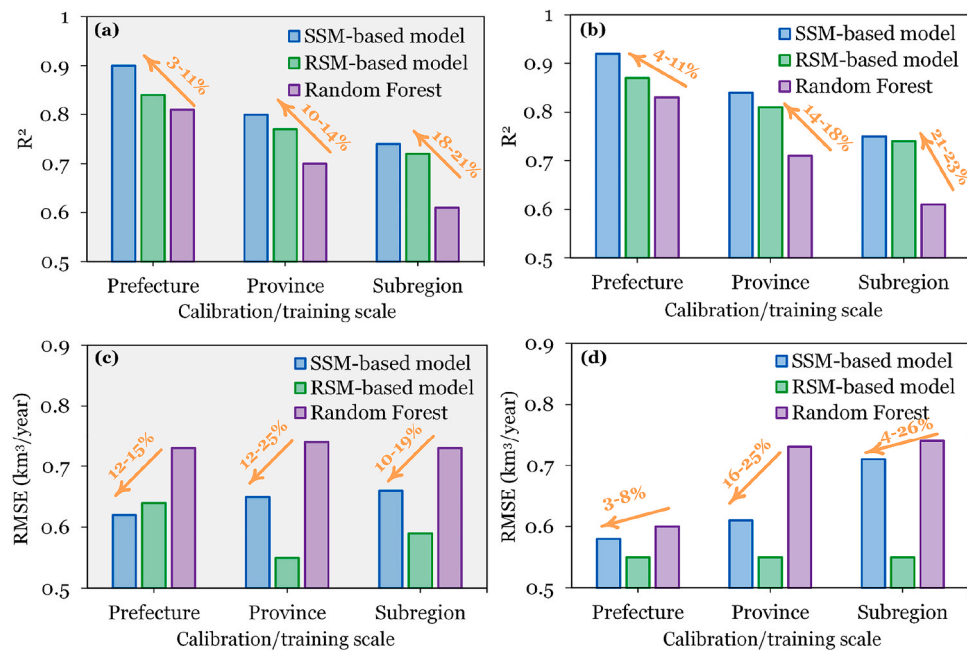
Fig. 6. Comparison of the performance of our IWU models with the Random Forest algorithm during the validation period (2010–2020). The left and right panels present results for two calibration/training periods (2001–2005 and 2001–2020, respectively). Each panel shows model performance when calibrated/trained at the prefectural, provincial, and subregional levels.
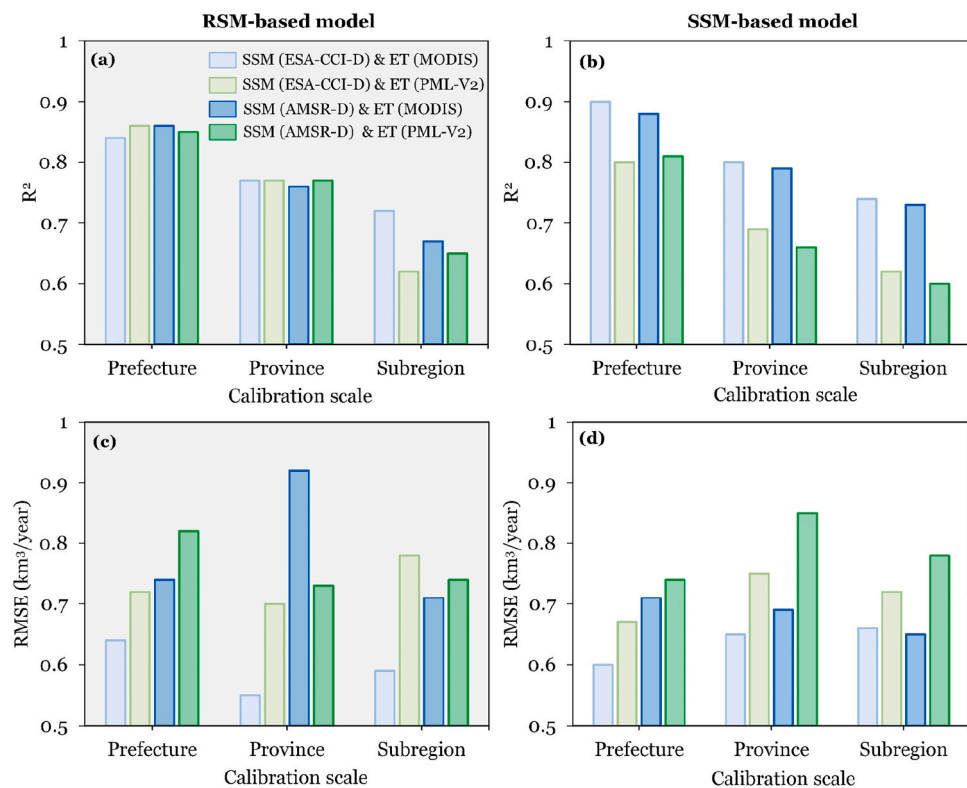

Fig. 7. Model performance using different satellite-based SSM and ET products. The left and right panels show the evaluation results for the RSM-based and SSM-based models, respectively, during the validation period (2010–2020). All models were calibrated at the prefectural, provincial and subregional levels, respectively, for the period 2001–2005.

reducing RMSE by up to 18 % and 28 % for the RSM- and SSM-based models, respectively. For the RSM-based model, the ensemble IWU estimates consistently exhibit higher R^2 values than any individual ensemble member, although their RMSE is slightly greater than that of

the best-performing member (i.e., the model driven by ESA-CCI-D SSM and MODIS ET). In contrast, for the SSM-based model, the ensemble estimates achieve R^2 values comparable to the best-performing member while maintaining consistently lower RMSE across all combinations.
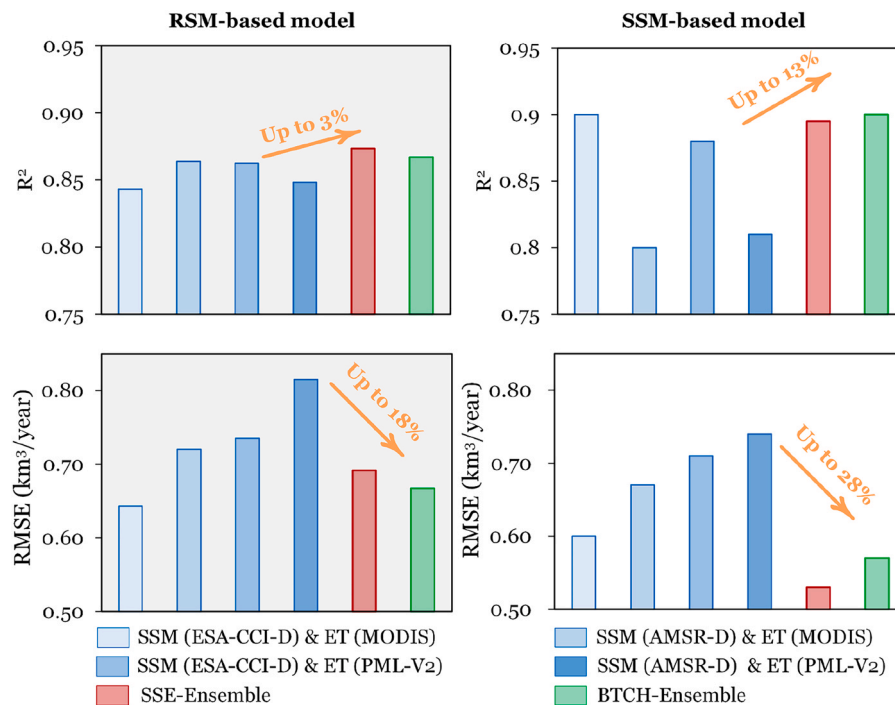
Fig. 8. Comparison of ensemble IWU estimation accuracy with models driven by different satellite-based products. Left and right panels present results for the RSM- and SSM-based models, respectively. "SSE-Ensemble" and "BTCH-ensemble" refer to the ensemble IWU estimates using the summed square error and the Bayesian Three-Cornered Hat methods, respectively. All models were calibrated at the prefectural level for 2001–2005, and their accuracy, along with the performance of the ensemble techniques, was evaluated for 2010–2020.

Overall, these results underscore the added value of ensemble approaches in enhancing the accuracy of IWU estimation.

3.4. Accuracy assessment of ensemble IWU estimates in China

By integrating the SSM-based model with the summed squared error (SSE) ensemble technique, we generated 1 km resolution ensemble IWU estimates across China for the period 2001–2020. As shown in Fig. 9, these estimates show strong agreement with prefecture-level reports used for model calibration, achieving an R^2 of 0.95, an RMSE of 0.27 km^3/year, and a bias of 0.07 km^3/year. When validated against independent IWU reports not used in model calibration, our estimates demonstrate high accuracy across multiple spatial scales, with R^2 values of 0.99, 0.93, and 0.89 for China's 10 major river basins, 21 subbasins, and 125 sub-prefectural (county-level) units, respectively. The corresponding RMSE values range from 0.07 to 4.91 km^3/year, and bias ranges from 0.02 to 3.22 km^3/year, depending on the IWU magnitude at each spatial scale. Collectively, these results highlight the robust performance of our ensemble IWU estimates.

As illustrated in Fig. 10, our IWU estimates demonstrate reasonable spatial agreement with IWU-Huang and IWU-Zhang, with Pearson correlation coefficients exceeding 0.60 (Supplementary Table S3). In contrast, agreement with IWU-Cheng is lower, likely due to its indirect estimation approach based on consumptive irrigation water use and irrigation efficiency (Chen et al., 2019). Despite these differences, all datasets consistently capture China's major irrigation hotspots, including northwestern China and the Hetao, Qingtongxia, and Dujiangyan irrigation districts. However, existing IWU products suffer from coarse spatial resolution (≥0.25°) and tend to underestimate IWU in several regions. For example, IWU-Cheng notably underestimates IWU in southern China, while IWU-Zhang underestimates it in the northwest. Furthermore, all existing products underestimate IWU in northeastern China, where paddy rice cultivation, characterized by high irrigation demand, is widespread (Supplementary Figure S7). The strong spatial similarity among existing IWU products primarily stems from

their shared reliance on the FAO Global Map of Irrigation Areas (Siebert et al., 2005). Although the FAO map provides globally consistent irrigation data, its accuracy in China is considerably lower than that of China-specific datasets CIrrMap250 (Zhang et al., 2022b). Consequently, our IWU estimates achieve markedly higher accuracy than existing products when validated against both dependent and independent statistical reports (Supplementary Figure S8).

3.5. Temporal patterns of IWU across China

As shown in Fig. 11a, China's IWU exhibited a clear increasing trend during 2001–2020, rising from 339 to 395 km^3/year, with an average of 360 km^3/year. Comparison with changes in irrigated area and water use intensity (i.e., IWU per unit irrigated area) indicates that the increasing trend in IWU was primarily driven by the expansion of irrigated area, while its interannual variability was largely controlled by fluctuations in water use intensity. The national average water use intensity was approximately 425 mm/year and showed a declining trend, which partially offset the overall increase in total IWU. The intra-annual variation of IWU closely mirrors China's agricultural calendar (Fig. 11b). IWU remains minimal during the cold dormant season (December-February), rises sharply in spring, and peaks during the active summer growing season (June-September). Spatially, the trend in IWU is highly heterogeneous (Fig. 11c). Significant increases occurred in Northeast and Northwest China, mainly due to the expansion of irrigated cropland (Supplementary Figure S9). In contrast, many southeastern provinces and localized areas elsewhere showed declines driven mainly by reduced water use intensity. In many regions, irrigated area and water use intensity displayed opposing trends, suggesting a trade-off effect in their combined influence on IWU.
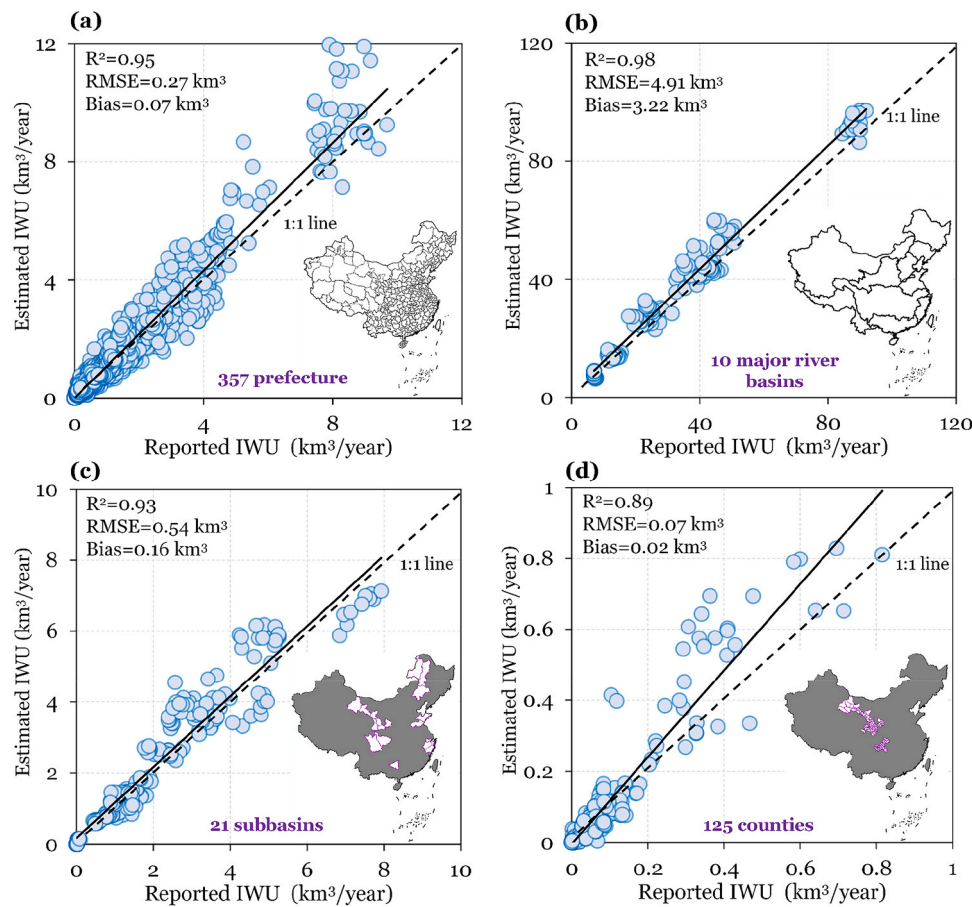
Fig. 9. Accuracy assessment of our ensemble IWU estimates against dependent and independent IWU reports. "Dependent" refers to IWU reports used in model calibration, whereas "independent" refers to reports excluded from the calibration process.

4. Discussion

4.1. Comparison with existing studies

We compared our methods and results with those of 31 recent studies that estimate IWU using remote sensing data (Supplementary Table S1). As shown in Supplementary Figure S10a, the cumulative number of such publications has increased sharply since 2018, reflecting both rapid methodological advances and growing research interest in remote sensing-based IWU estimation. Among the reviewed studies, 47 % employed ET-based methods, 44 % used soil moisture (SM)-based approaches, and only 9 % adopted a combined SM-ET approach. Notably, many ET-based methods could not be validated against consumptive irrigation water use because such reference data are generally unavailable. Regarding spatial scales, 47 % of the studies were conducted at the field or plot level (Supplementary Figure S10b), 32 % at the basin or district scale, and the remaining 20 % at national or global scales. Large-scale IWU estimation remains challenging due to limited ground observations for calibration and validation, the coarse resolution and uncertainties of remote sensing products, and the strong spatial and temporal heterogeneity of irrigation practices. Against this background, our model, which integrates both SM and ET information, demonstrates strong applicability at the national scale across China, representing a unique contribution to remote sensing-based IWU estimation methodologies.

We further compared the performance of our model with that reported in previous studies reporting R^2 values (n = 17 out of 31). As shown in Supplementary Figure S10c, reported R^2 values vary widely, from 0.3 to 1.0, with most below 0.70, lower than the performance achieved by our RSM- and SSM-based models. Because of scale differences, direct comparisons with field- or basin-scale studies are not straightforward; therefore, we focused on large-scale (national or global) studies. Two global-scale studies employed SM-based approaches to generate IWU estimates at 10 or 25 km resolution, which exhibited systematic underestimations ranging from 3.1 to 77 km^3 /year (Zohaib and Choi, 2020; Zhang et al., 2022a). These underestimations mainly result from the coarse resolution of SM products, which fail to capture localized irrigation signals, and the reliance on static irrigated area maps that overlook irrigation expansion. Chen et al. (2019) developed an ET-based approach to estimate global IWU at 10 km resolution and reported near-perfect agreement with FAO-reported national values. However, our evaluation indicates that their estimates perform poorly at the sub-national scale in China (Supplementary Figure S8). In the United States, Zhang and Long (2021) proposed a new SM-ET combined approach to make spatially explicit estimates of IWU with higher accuracy and finer resolution than those derived from SM-based methods (Zaussinger et al., 2019). Compared with Zhang and Long (2021), our framework attains higher accuracy in China because it is explicitly calibrated against IWU reports.

4.2. Reliability and uncertainties of IWU reports

Although prefecture-level IWU reports provide an essential reference for model calibration and validation, they are not derived solely from direct field measurements. In China, the official IWU statistics published in the Water Resources Bulletins are compiled through a combination of comprehensive and representative surveys conducted by local water resource authorities (Shen et al., 2020). For large irrigation districts,
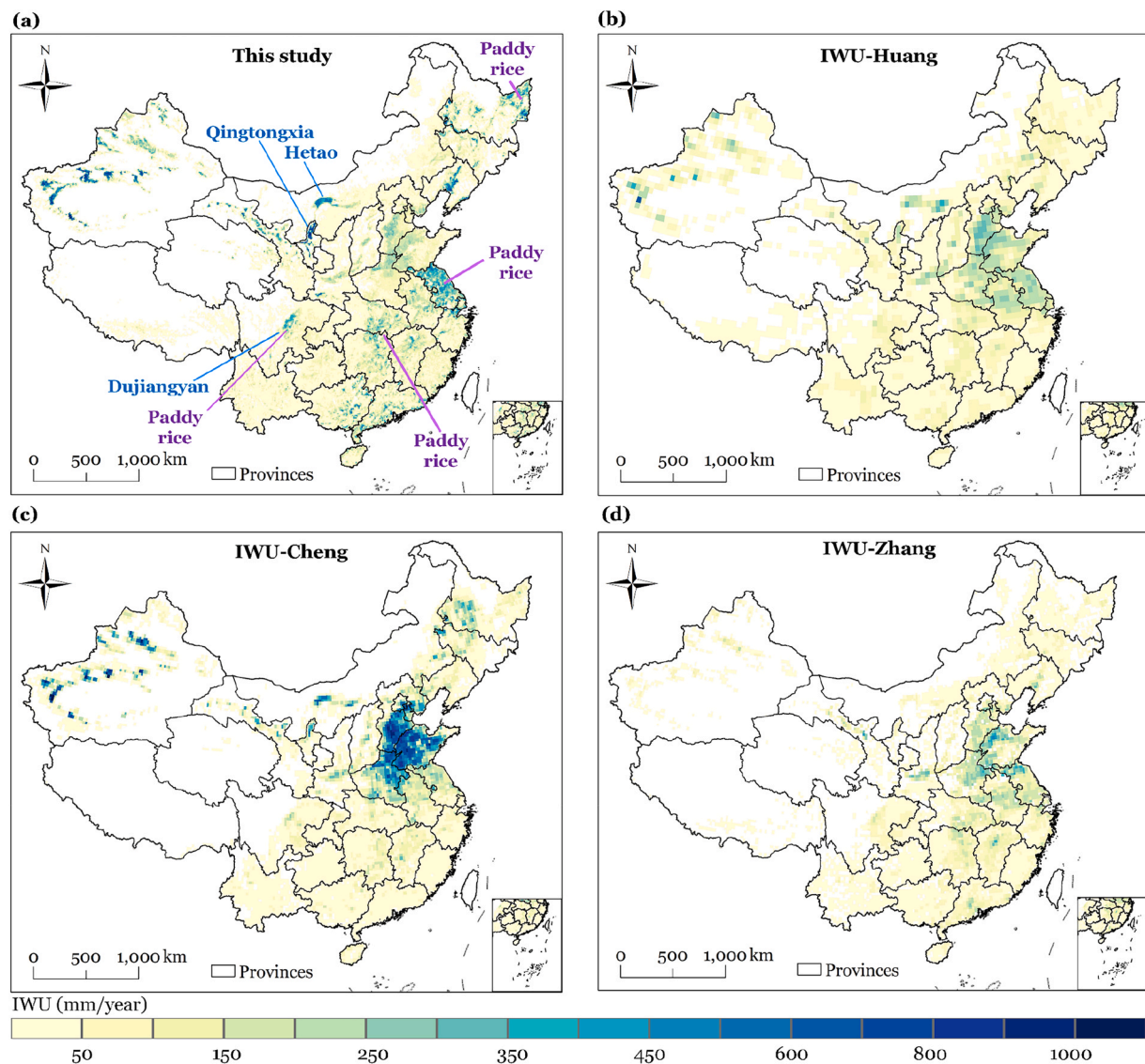
Fig. 10. Spatial comparison of our ensemble IWU estimates (a) with existing products: IWU-Huang (b), IWU-Cheng (c), and IWU-Zhang (d).

irrigation withdrawals are either directly metered at intake points or obtained from dispatch and management records. For small and scattered irrigation areas, water use per unit area is estimated based on field surveys or regional irrigation quotas, and total IWU is then obtained by multiplying these values by the actual irrigated area. These data are subsequently aggregated across administrative levels (from county to prefecture) and quality-controlled by the Ministry of Water Resources. As a result, the IWU reports combine both measured and survey-based information, differing fundamentally from the estimates produced by the satellite-driven modeling framework developed in this study.

Nevertheless, several sources of uncertainty are inherent in these statistical datasets. First, the representativeness of surveys and the accuracy of irrigation quotas may vary regionally, potentially introducing bias into estimated IWU values (Shen et al., 2016). Second, IWU compilation involves multiple governmental departments using heterogeneous statistical methods and definitions, occasionally resulting in inconsistencies or duplicated accounting. Third, in complex irrigation systems, such as those with mixed groundwater-surface water sources or dense canal networks, accurate quantification of water use remains technically challenging. These limitations suggest that the reported IWU should be regarded as the best available estimates rather than precise ground-truth measurements. Despite these uncertainties, the IWU

statistics remain the most reliable and widely recognized dataset currently available for large-scale irrigation assessments in China (Zhou et al., 2020a; Zhang et al., 2022a; Liu et al., 2024a).

4.3. Pros, cons, and uncertainties of our IWU estimation framework

Our method integrates both satellite-derived ET and soil moisture (SM) information, with parameters calibrated against census-based IWU reports. This integration likely explains its superior performance compared with approaches that rely solely on ET or SM, as neither can independently capture irrigation inputs. The framework addresses key shortcomings of SM-based methods, which tend to underestimate IWU, and ET-based approaches, which require uncertain irrigation efficiency parameters. Compared with existing SM-ET methods (Hu et al., 2016; Zhang and Long, 2021), our framework avoids dependence on fixed empirical models for quantifying irrigation components (e.g., drainage losses), thereby enhancing its adaptability and transferability across regions. Furthermore, it eliminates the need to develop and calibrate high-resolution hydrological models under rainfed conditions (Kragh et al., 2023a), a process that is both challenging and time-consuming at large scales.

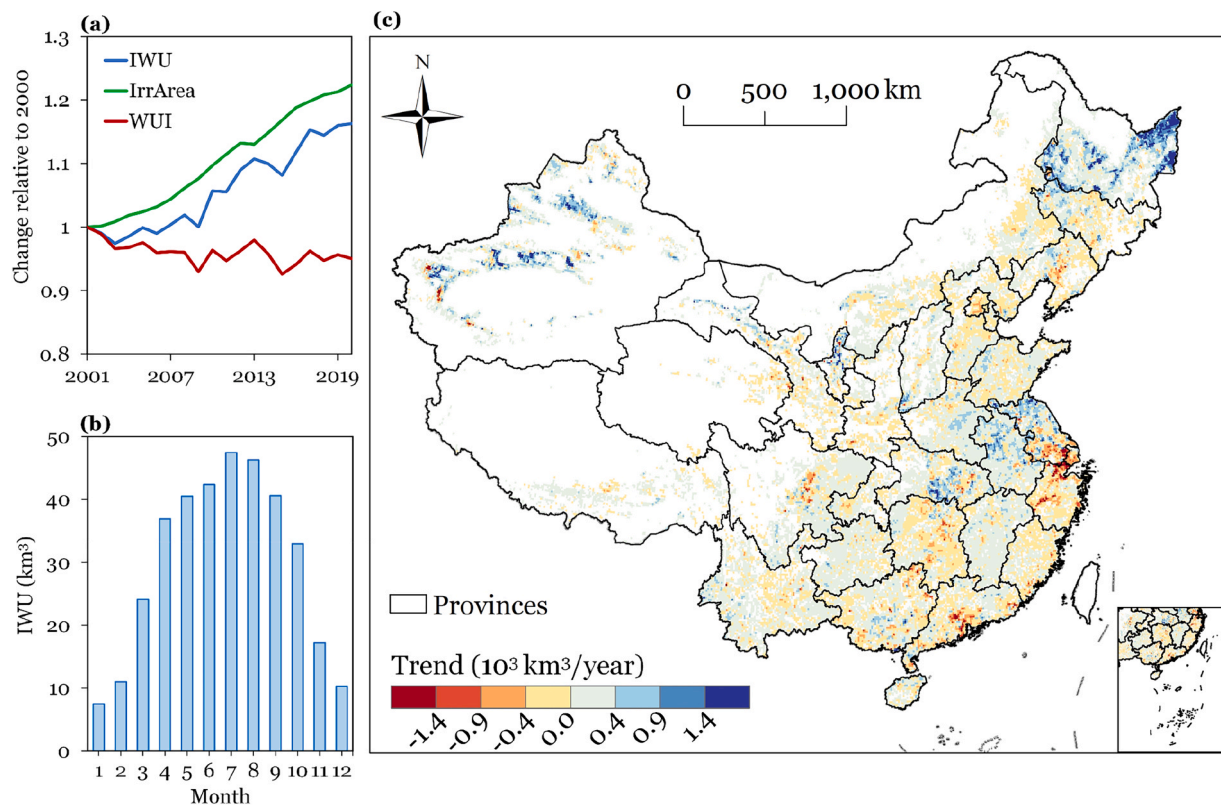In regions with census data, our framework adds value beyond

Fig. 11. Temporal patterns of IWU across China. Panel (a) illustrates the interannual variations in IWU, irrigated area (IrrArea), and water use intensity (WUI, defined as IWU per unit irrigated area), each normalized to their respective values in 2001. Panel (b) presents the intra-annual distribution of IWU, while the panel (c) depicts the spatial distribution of linear IWU trends during 2001–2020 at the grid scale.

administrative statistics, which typically provide only aggregated IWU at coarse administrative levels. By integrating remote sensing and reanalysis datasets within a physically based model, it produces spatially explicit IWU estimates at fine resolution (e.g., 1 km), which are essential for refined water allocation, sustainable irrigation assessment, and hydroclimatic impact analyses (Dari et al., 2024). The framework can also reconstruct IWU dynamics at sub-annual (e.g., monthly) scales and predict irrigation withdrawals during periods without census data. In regions lacking census data, the framework may be extended through a two-step strategy: first, estimating aggregated IWU using a machine learning-based metamodel and globally available datasets (Kragh et al., 2025); and second, calibrating our model with these aggregated estimates to produce physically consistent and spatially explicit IWU fields.

Nevertheless, several limitations and sources of uncertainty remain. First, the method is not calibration-free; it requires IWU observations or reports for parameter optimization. Unlike SM2RAIN-based methods, which calibrate parameters using more reliable references such as precipitation (Brocca et al., 2018; Dari et al., 2022, 2023b), our approach relies on IWU statistics that are typically aggregated regionally at annual scales and carry inherent uncertainties, limiting high spatiotemporal resolution calibration. Second, the method does not explicitly account for groundwater contributions to ET. In areas with shallow water tables, particularly arid regions, groundwater can substantially increase irrigation water consumption (Gao et al., 2017, 2018). Meanwhile, flooded croplands (e.g., paddy rice) are simplified as a single-layer soil system, neglecting key processes such as pond water storage and surface runoff inherent to a two-layer (pond-soil) structure. This simplification may reduce physical interpretability, although it can implicitly capture the high irrigation demand required to maintain the ponded layer via combined ET and drainage effects.

Lastly, the model's performance is strongly dependent on the quality of remote sensing inputs. Downscaled soil moisture datasets can carry

large uncertainties and often poorly represent site-level water dynamics (Beck et al., 2021). Agricultural practices, such as tillage and tile drainage, further influence soil water behavior, yet these anthropogenic effects are generally not represented in satellite-based soil moisture retrievals. Furthermore, satellite-based ET products tend to underestimate ET over irrigated croplands, as they rarely account explicitly for irrigation events (Zhu et al., 2019; Liu et al., 2024b) (Supplementary Figure S11). These uncertainties affect both IWU accuracy and the model's partitioning of irrigation losses. Our model attributes 77 % of total irrigation water to drainage, 20 % to ET, and 3 % to surface soil moisture storage. The disproportionately high drainage fraction likely reflects the combined effects of underestimated ET (Zhang and Long, 2021) and the absence of explicit representation of conveyance losses. Model calibration likely compensated for these factors by allocating a larger fraction of water to drainage, thereby maintaining consistency with reported IWU values.

5. Conclusions

Irrigation plays a crucial role in both food production and Earth system dynamics, making the spatially explicit estimation of irrigation water use (IWU) a high-priority research topic in the fields of remote sensing, agriculture, and hydrology. This study addresses the challenges of large-scale, high-resolution IWU estimation by developing a novel, physically based, and generalizable framework. The framework integrates satellite-derived soil moisture and evapotranspiration products with reanalysis data using soil water balance principles to generate spatially explicit IWU estimates. When applied across China, the framework demonstrated satisfactory accuracy and exhibited greater stability and robustness compared to the widely used Random Forest algorithm. The methodology is transferable to other regions, and the resulting dataset provides valuable insights into IWU dynamics in China,

offering substantial support for agricultural, hydrological, and climate research, as well as sustainable water management.

CRediT authorship contribution statement

Xin Li: Writing – review & editing, Resources, Funding acquisition. **Donghai Zheng:** Writing – review & editing, Resources, Methodology. **Kun Zhang:** Writing – review & editing, Validation, Methodology. **Tao Che:** Writing – review & editing, Supervision, Funding acquisition, Conceptualization. **Ling Zhang:** Writing – review & editing, Writing – original draft, Resources, Methodology, Funding acquisition, Formal analysis, Data curation, Conceptualization.

Declaration of Competing interest

The authors declare that they have no known competing financial interests or personal relationships that could have appeared to influence the work reported in this paper.

Acknowledgements

Appendix A. Supporting information

Supplementary data associated with this article can be found in the online version at doi:10.1016/j.agwat.2025.110077.

Data availability

Data will be made available on request.

References

Abolafia Rosenzweig, R., Livneh, B., Small, E.E., Kumar, S.V., 2019. Soil moisture data assimilation to estimate irrigation water use. J. Adv. Model. Earth Syst. 11, 3670–3690. https://doi.org/10.1029/2019MS001797.

Alkon, M., Wang, Y., 2024. High resolution prediction and explanation of groundwater depletion across India. Environ. Res. Lett. 19 (4), 044072.

Beck, H.E., Pan, M.W., Miralles, D.G., Reichle, R.H., Dorigo, W.A., Hahn, S., Sheffield, J., Karthikeyan, L., Balsamo, G., Parinussa, R.M., van Dijk, A.I.J.M., Du, J., Kimball, J. S., Vergopolan, N., Wood, E.F., 2021. Evaluation of 18 satellite- and model-based soil moisture products using in situ measurements from 826 sensors. Hydrol. Earth Syst. Sci. 25 (1), 17–40. https://doi.org/10.5194/hess-25-17-2021.

Bhattarai, N., Pollack, A., Lobell, D.B., Fishman, R., Singh, B., Dar, A., Jain, M., 2021. The impact of groundwater depletion on agricultural production in India. Environ. Res. Lett. 16 (8), 085003. https://doi.org/10.1088/1748-9326/ac10de.

Bo, Y., Li, X., Liu, K., Wang, S., Li, D., Xu, Y., Wang, M., 2024. Hybrid theory-guided data driven framework for calculating irrigation water use of three staple cereal crops in China. Water Resour. Res. 60 (3), e2023WR035234. https://doi.org/10.1029/2023WR035234.

Boser, A., Caylor, K., Larsen, A., Pascolini-Campbell, M., Reager, J.T., Carleton, T., 2024. Field-scale crop water consumption estimates reveal potential water savings in California agriculture. Nat. Commun. 15 (1), 2366. https://doi.org/10.1038/s41467-024-46031-2.

Breiman, L., 2001. Random forests. Mach. Learn. 45 (1), 5–32. https://doi.org/10.1023/A:1010933404324.

Brocca, L., Moramarco, T., Melone, F., Wagner, W., 2013. A new method for rainfall estimation through soil moisture observations. Geophys. Res. Lett. 40 (5), 853–858. https://doi.org/10.1002/grl.50173.

Brocca, L., Tarpanelli, A., Filippucci, P., Dorigo, W., Zaussinger, F., Gruber, A., Fernández-Prieto, D., 2018. How much water is used for irrigation? A new approach exploiting coarse resolution satellite soil moisture products. Int. J. Appl. Earth Obs. Geoinf. 73, 752–766. https://doi.org/10.1016/j.jag.2018.08.023.

Brombacher, J., Silva, I.R.D.O., Degen, J., Pelgrum, H., 2022. A novel evapotranspiration based irrigation quantification method using the hydrological similar pixels algorithm. Agric. Water Manag. 267, 107602. https://doi.org/10.1016/j.agwat.2022.107602.

Brookfield, A.E., Zipper, S., Kendall, A.D., Ajami, H., Deines, J.M., 2023. Estimating groundwater pumping for irrigation - a method comparison. Groundwater 62, 15–33. https://doi.org/10.1111/gwat.13336.

Busschaert, L., Bechtold, M., Modanesi, S., Massari, C., Brocca, L., De Lannoy, G.J.M., 2024. Irrigation quantification through backscatter data assimilation with a buddy check approach. J. Adv. Model. Earth Syst. 16 (3), e2023MS003661. https://doi.org/10.1029/2023MS003661.

Cheema, M.J.M., Immerzeel, W.W., Bastiaanssen, W.G.M., 2014. Spatial quantification of groundwater abstraction in the irrigated Indus basin. Groundwater 52 (1), 25–36. https://doi.org/10.1111/gwat.12027.

Chen, Y., Feng, X., Fu, B., Shi, W., Yin, L., Lv, Y., 2019. Recent global cropland water consumption constrained by observations. Water Resour. Res. 55, 3708–3738. https://doi.org/10.1029/2018WR023573.

Dari, J., Brocca, L., Modanesi, S., Massari, C., Tarpanelli, A., Barbetta, S., Quast, R., Vreugdenhil, M., Freeman, V., Barella-Ortiz, A., Quintana-Seguí, P., Bretreger, D., Volden, E., 2023a. Regional data sets of high-resolution (1 and 6 km) irrigation estimates from space. Earth Syst. Sci. Data 15 (4), 1555–1575. https://doi.org/10.5194/essd-15-1555-2023.

Dari, J., Brocca, L., Modanesi, S., Massari, C., Tarpanelli, A., Barbetta, S., Quast, R., Vreugdenhil, M., Freeman, V., Barella-Ortiz, A., Quintana-Seguí, P., Bretreger, D., Volden, E., 2023b. Regional data sets of high-resolution (1 and 6km) irrigation estimates from space. Earth Syst. Sci. Data 15 (4), 1555–1575. https://doi.org/10.5194/essd-15-1555-2023.

Dari, J., Quintana-Seguí, P., Barella-Ortiz, A., Rahmati, M., Saltalippi, C., Flammini, A., Brocca, L., 2024. Quantifying the hydrological impacts of irrigation on a mediterranean agricultural context through explicit satellite-derived irrigation estimates. Water Resour. Res. 60 (5), e2023WR036510. https://doi.org/10.1029/2023WR036510.

Dari, J., Quintana-Seguí, P., Morbidelli, R., Saltalippi, C., Flammini, A., Giugliarelli, E., Escorihuela, M.J., Stefan, V., Brocca, L., 2022. Irrigation estimates from space: implementation of different approaches to model the evapotranspiration contribution within a soil-moisture-based inversion algorithm. Agric. Water Manag. 265, 107537. https://doi.org/10.1016/j.agwat.2022.107537.

Döll, P., Siebert, S., 2002. Global modeling of irrigation water requirements, 8-1 Water Resour. Res. 38 (4), 8–10. https://doi.org/10.1029/2001WR000355.

Driscoll, A.W., Conant, R.T., Marston, L.T., Choi, E., Mueller, N.D., 2024. Greenhouse gas emissions from US irrigation pumping and implications for climate-smart irrigation policy. Nat. Commun. 15 (1), 675. https://doi.org/10.1038/s41467-024-44920-0.

van Eekelen, M.W., Bastiaanssen, W.G.M., Jarmain, C., Jackson, B., Ferreira, F., van der Zaag, P., Saraiva Okello, A., Bosch, J., Dye, P., Bastidas-Obando, E., Dost, R.J.J., Luxemburg, W.M.J., 2015. A novel approach to estimate direct and indirect water withdrawals from satellite measurements: a case study from the Incomati basin. Agric. Ecosyst. Environ. 200, 126–142. https://doi.org/10.1016/j.agee.2014.10.023.

FAO, 2006. Global Information System on Water and Agriculture: Irrigated crop calendars (⟨https://www.fao.org/aquastat/en/data-analysis/irrig-water-use/irrigated-crop-calendars⟩).

Filippelli, S.K., Sloggy, M.R., Vogeler, J.C., Manning, D.T., Goemans, C., Senay, G.B., 2022. Remote sensing of field-scale irrigation withdrawals in the central Ogallala aquifer region. Agric. Water Manag. 271, 107764. https://doi.org/10.1016/j.agwat.2022.107764.

Filippucci, P., Tarpanelli, A., Massari, C., Serafini, A., Strati, V., Alberi, M., Raptis, K.G. C., Mantovani, F., Brocca, L., 2020. Soil moisture as a potential variable for tracking and quantifying irrigation: a case study with proximal gamma-ray spectroscopy data. Adv. Water Resour. 136, 103502. https://doi.org/10.1016/j.advwatres.2019.103502.

Ford, T.W., Harris, E., Quiring, S.M., 2014. Estimating root zone soil moisture using near-surface observations from SMOS. Hydrol. Earth Syst. Sci. 18 (1), 139–154. https://doi.org/10.5194/hess-18-139-2014.

Foster, T., Gonçalves, I.Z., Campos, I., Neale, C.M.U., Brozović, N., 2019. Assessing landscape scale heterogeneity in irrigation water use with remote sensing and in situ monitoring. Environ. Res. Lett. 14 (2), 24004. https://doi.org/10.1088/1748-9326/aaf2be.

Foster, T., Mieno, T., Brozovic, N., 2020. Satellite-based monitoring of irrigation water use: assessing measurement errors and their implications for agricultural water management policy. Water Resour. Res. 56, e2020WR028378. https://doi.org/10.1029/2020WR028378.

Gao, X., Bai, Y., Huo, Z., Xu, X., Huang, G., Xia, Y., Steenhuis, T.S., 2017. Deficit irrigation enhances contribution of shallow groundwater to crop water consumption in arid area. Agric. Water Manag. 185, 116–125. https://doi.org/10.1016/j.agwat.2017.02.012.

Gao, X., Huo, Z., Xu, X., Qu, Z., Huang, G., Tang, P., Bai, Y., 2018. Shallow groundwater plays an important role in enhancing irrigation water productivity in an arid area: the perspective from a regional agricultural hydrology simulation. Agric. Water Manag. 208, 43–58. https://doi.org/10.1016/j.agwat.2018.06.009.

Han, F., Zheng, Y., Zhang, L., Xiong, R., Hu, Z., Tian, Y., Li, X., 2023. Simulating drip irrigation in large-scale and high-resolution ecohydrological models: from emitters to the basin. Agric. Water Manag. 289, 108500. https://doi.org/10.1016/j.agwat.2023.108500.

Hargreaves, G.H., 1994. Defining and using reference evapotranspiration. J. Irrig. Drain. Eng. 120 (6), 1132–1139. https://doi.org/10.1061/(ASCE)0733-9437(1994)120:6(1132).

He, X., Xu, T., Xia, Y., Bateni, S.M., Guo, Z., Liu, S., Mao, K., Zhang, Y., Feng, H., Zhao, J., 2020. A Bayesian three-cornered hat (BTCH) method: improving the terrestrial evapotranspiration estimation. Remote Sens. 12 (5). https://doi.org/10.3390/rs12050878.

He, S., Zhang, Y., Ma, N., Tian, J., Kong, D., Liu, C., 2022. A daily and 500 m coupled evapotranspiration and gross primary production product across China during 2000-2020. Earth Syst. Sci. Data 14, 5463–5488. https://doi.org/10.5194/essd-2022-183.

Hu, X., Shi, L., Zeng, J., Yang, J., Zha, Y., Yao, Y., Cao, G., 2016. Estimation of actual irrigation amount and its impact on groundwater depletion: a case study in the Hebei Plain, China. J. Hydrol. 543, 433–449. https://doi.org/10.1016/j.jhydrol.2016.10.020.

Hu, Y., Zhang, L., Zhao, Y., Che, T., 2024. ChinaMet: a multisource integrated high-resolution multi-variable meteorological dataset for China [Data set]. Zenodo. https://doi.org/10.5281/zenodo.14580706.

Huang, Z., Hejazi, M., Li, X., Tang, Q., Vernon, C., Leng, G., Liu, Y., Doell, P., Eisner, S., Gerten, D., Hanasaki, N., Wada, Y., 2018. Reconstruction of global gridded monthly sectoral water withdrawals for 1971–2010 and analysis of their spatiotemporal patterns. Hydrol. Earth Syst. Sci. 22, 2117–2133. https://doi.org/10.5194/hess-22-2117-2018.

Huang, G., Hoekstra, A.Y., Krol, M.S., Jägermeyr, J., Galindo, A., Yu, C., Wang, R., 2020. Water-saving agriculture can deliver deep water cuts for China. Resour. Conserv. Recycl. 154, 104578. https://doi.org/10.1016/j.resconrec.2019.104578.

Jägermeyr, J., Gerten, D., Heinke, J., Schaphoff, S., Kummu, M., Lucht, W., 2015. Water savings potentials of irrigation systems: global simulation of processes and linkages. Hydrol. Earth Syst. Sci. 19 (7), 3073–3091. https://doi.org/10.5194/hess-19-3073-2015.

Jalilvand, E., Abolafia Rosenzweig, R., Tajrishy, M., Kumar, S.V., Mohammadi, M.R., Das, N.N., 2023. Is it possible to quantify irrigation water-use by assimilating a high-resolution satellite soil moisture product? Water Resour. Res. 59 (4), e2022WR033342. https://doi.org/10.1029/2022WR033342.

Jung, H., Saynisch-Wagner, J., Schulz, S., 2024. Can explainable AI offer a new perspective for groundwater recharge estimation?-global-scale modeling using neural network. Water Resour. Res. 60 (4), e2023WR036360. https://doi.org/10.1029/2023WR036360.

Kebede, E.A., Oluoch, K.O.A., Siebert, S., Mehta, P., Hartman, S., Jägermeyr, J., Ray, D., Ali, T., Brauman, K.A., Deng, Q., Xie, W., Davis, K.F., 2025. A global open-source dataset of monthly irrigated and rainfed cropped areas (MIRCA-OS) for the 21st century. Sci. Data 12 (1), 208. https://doi.org/10.1038/s41597-024-04313-w.

Koch, J., Zhang, W., Martinsen, G., He, X., Stisen, S., 2020. Estimating net irrigation across the North China Plain through dual modelling of evapotranspiration. Water Resour. Res. 56, e2020WR027413. https://doi.org/10.1029/2020WR027413.

Kragh, S.J., Dari, J., Modanesi, S., Massari, C., Brocca, L., Fensholt, R., Stisen, S., Koch, J., 2023a. An inter-comparison of approaches and frameworks to quantify irrigation from satellite data. Hydrol. Earth Syst. Sci. 28, 441–457. https://doi.org/10.5194/hess-2023-142.

Kragh, S.J., Fensholt, R., Stisen, S., Koch, J., 2023b. The precision of satellite-based net irrigation quantification in the Indus and Ganges basins. Hydrol. Earth Syst. Sci. 27 (13), 2463–2478. https://doi.org/10.5194/hess-27-2463-2023.

Kragh, S.J., Schneider, R., Fensholt, R., Stisen, S., Koch, J., 2025. Synthesizing regional irrigation data using machine learning – towards global upscaling via metamodeling. Agric. Water Manag. 311, 109404. https://doi.org/10.1016/j.agwat.2025.109404.

Laluet, P., Olivera-Guerra, L.E., Altés, V., Paolini, G., Ouaadi, N., Rivalland, V., Jarlan, L., Villar, J.M., Merlin, O., 2024. Retrieving the irrigation actually applied at district scale: assimilating high-resolution Sentinel-1-derived soil moisture data into a FAO-56-based model. Agric. Water Manag. 293, 108704. https://doi.org/10.1016/j.agwat.2024.108704.

Li, X., Long, D., Slater, L.J., Moulds, S., Shahid, M., Han, P., Zhao, F., 2023. Soil moisture to runoff (SM2R): a data-driven model for runoff estimation across poorly gauged asian water towers based on soil moisture dynamics. Water Resour. Res. 59 (3), e2022WR033597. https://doi.org/10.1029/2022WR033597.

Liu, K., Bo, Y., Li, X., Wang, S., Zhou, G., 2024a. Uncovering current and future variations of irrigation water use across China using machine learning. Earth's. Future 12 (3), e2023EF003562. https://doi.org/10.1029/2023EF003562.

Liu, Y., Li, F., Zhao, Y., 2024b. Improved hydrological modelling and ET estimation in watershed with irrigation interference. J. Hydrol. 634, 131108. https://doi.org/10.1016/j.jhydrol.2024.131108.

Lu, B., Liu, C., Meng, X., Zhang, Z., Herrmann, H., Li, X., 2023. High-resolution mapping of regional NMVOCs using the fast space-time light gradient boosting machine (LightGBM). J. Geophys. Res. Atmospheres 128 (22), e2023JD039591. https://doi.org/10.1029/2023JD039591.

Ma, D., Bortnik, J., Chu, X., Claudepierre, S.G., Ma, Q., Kellerman, A., 2023. Opening the Black Box of the radiation belt machine learning model. Space Weather 21 (4), e2022SW003339. https://doi.org/10.1029/2022SW003339.

Majumdar, S., Smith, R., Butler, J.J., Lakshmi, V., 2020. Groundwater withdrawal prediction using integrated multi-temporal remote sensing datasets and machine learning. Water Resour. Res. 56, e2020WR028059. https://doi.org/10.1029/2020WR028059.

Majumdar, S., Smith, R., Conway, B.D., Lakshmi, V., 2022. Advancing remote sensing and machine learning-driven frameworks for groundwater withdrawal estimation in Arizona: linking land subsidence to groundwater withdrawals. Hydrol. Process. 36 (11), e14757. https://doi.org/10.1002/hyp.14757.

McDermid, S., Nocco, M., Lawston-Parker, P., Keune, J., Pokhrel, Y., Jain, M., Jägermeyr, J., Brocca, L., Massari, C., Jones, A.D., Vahmani, P., Thiery, W., Yao, Y., Bell, A., Chen, L., Dorigo, W., Hanasaki, N., Jasechko, S., Lo, M.-H., Mahmood, R., Mishra, V., Mueller, N.D., Niyogi, D., Rabin, S.S., Sloat, L., Wada, Y., Zappa, L., Chen, F., Cook, B.I., Kim, H., Lombardozzi, D., Polcher, J., Ryu, D., Santanello, J., Satoh, Y., Seneviratne, S., Singh, D., Yokohata, T., 2023. Irrigation in the Earth system. Nat. Rev. Earth Environ. 4, 435–453. https://doi.org/10.1038/s43017-023-00438-5.

Mehta, P., Siebert, S., Kummu, M., Deng, Q., Ali, T., Marston, L., Xie, W., Davis, K.F., 2024. Half of twenty-first century global irrigation expansion has been in water-stressed regions. Nat. Water 2 (3), 254–261. https://doi.org/10.1038/s44221-024-00206-9.

Monteith, J.L., 1965. Evaporation and environment. Symposia of the Society for Experimental Biology. Cambridge University Press (CUP), Cambridge, pp. 205–234.

Mu, Q., Zhao, M., Running, S.W., 2011. Improvements to a MODIS global terrestrial evapotranspiration algorithm. Remote Sens. Environ. 115 (8), 1781–1800. https://doi.org/10.1016/j.rse.2011.02.019.

Muñoz-Sabater, J., Dutra, E., Agustí-Panareda, A., Albergel, C., Arduini, G., Balsamo, G., Boussetta, S., Choulga, M., Harrigan, S., Hersbach, H., Martens, B., Miralles, D.G., Piles, M., Rodríguez-Fernández, N.J., Zsoter, E., Buontempo, C., Thépaut, J.N., 2021. ERA5-Land: a state-of-the-art global reanalysis dataset for land applications. Earth Syst. Sci. Data 13 (9), 4349–4383. https://doi.org/10.5194/essd-13-4349-2021.

Olivera-Guerra, L.-E., Laluet, P., Altés, V., Ollivier, C., Pageot, Y., Paolini, G., Chavanon, E., Rivalland, V., Boulet, G., Villar, J.-M., Merlin, O., 2023. Modeling actual water use under different irrigation regimes at district scale: application to the FAO-56 dual crop coefficient method. Agric. Water Manag. 278, 108119. https://doi.org/10.1016/j.agwat.2022.108119.

Ott, T.J., Majumdar, S., Huntington, J.L., Pearson, C., Bromley, M., Minor, B.A., ReVelle, P., Morton, C.G., Sueki, S., Beamer, J.P., Jasoni, R.L., 2024. Toward field-scale groundwater pumping and improved groundwater management using remote sensing and climate data. Agric. Water Manag. 302, 109000. https://doi.org/10.1016/j.agwat.2024.109000.

Peña-Arancibia, J.L., Mainuddin, M., Kirby, J.M., Chiew, F.H.S., McVicar, T.R., Vaze, J., 2016. Assessing irrigated agriculture's surface water and groundwater consumption by combining satellite remote sensing and hydrologic modelling. Sci. Total Environ. 542, 372–382. https://doi.org/10.1016/j.scitotenv.2015.10.086.

Puy, A., Lankford, B., 2022. Large variations in global irrigation withdrawals caused by uncertain irrigation efficiencies. Environ. Res. Lett. 17 (4), 044014.

Qin, J., Duan, W., Zou, S., Chen, Y., Huang, W., Rosa, L., 2024. Global energy use and carbon emissions from irrigated agriculture. Nat. Commun. 15 (1), 3084. https://doi.org/10.1038/s41467-024-47383-5.

Qin, Y., Mueller, N.D., Siebert, S., Jackson, R.B., AghaKouchak, A., Zimmerman, J.B., Tong, D., Hong, C., Davis, S.J., 2019. Flexibility and intensity of global water use. Nat. Sustain. 2 (6), 515–523. https://doi.org/10.1038/s41893-019-0294-2.

Romaguera, M., Krol, M., Salama, M., Su, Z., Hoekstra, A., 2014a. Application of a remote sensing method for estimating monthly blue water evapotranspiration in irrigated agriculture. Remote Sens. 6 (10), 10033–10050. https://doi.org/10.3390/rs61010033.

Romaguera, M., Salama, M., Krol, M., Hoekstra, A., Su, Z., 2014b. Towards the improvement of blue water evapotranspiration estimates by combining remote sensing and model simulation. Remote Sens. 6 (8), 7026–7049. https://doi.org/10.3390/rs6087026.

Shangguan, W., Dai, Y., Liu, B., Zhu, A., Duan, Q., Wu, L., Ji, D., Ye, A., Yuan, H., Zhang, Q., Chen, D., Chen, M., Chu, J., Dou, Y., Guo, J., Li, H., Li, J., Liang, L., Liang, X., Liu, H., Liu, S., Miao, C., Zhang, Y., 2013. A China data set of soil properties for land surface modeling. J. Adv. Model. Earth Syst. 5 (2), 212–224. https://doi.org/10.1002/jame.20026.

Shen, Y., Chen, M., Cui, J., Zhang, S., Luo, Y., 2020. A study of the selection method of the sample irrigation area in agricultural irrigation water consumption statistics (in Chinese). China Rural Water Hydropower 4, 112–115.

Shen, Y., Zhang, S., Ji, Y., 2016. Determination of statistical methods and progress of work on agricultural irrigation water use in China (in Chinese). China Rural Water Hydropower 11, 133–134.

Siebert, S., Döll, P., Hoogeveen, J., Faures, J.M., Frenken, K., Feick, S., 2005. Development and validation of the global map of irrigation areas. Hydrol. Earth Syst. Sci. 9 (5), 535–547. https://doi.org/10.5194/hess-9-535-2005.

Siebert, S., Döll, P., 2010. Quantifying blue and green virtual water contents in global crop production as well as potential production losses without irrigation. J. Hydrol. 384 (3-4), 198–217. https://doi.org/10.1016/j.jhydrol.2009.07.031.

Song, P., Zhang, Y., Guo, J., Shi, J., Zhao, T., Tong, B., 2022. A 1 km daily surface soil moisture dataset of enhanced coverage under all-weather conditions over China in 2003–2019. Earth Syst. Sci. Data 14 (6), 2613–2637. https://doi.org/10.5194/essd-14-2613-2022.

UNESCO World Water Assessment Programme, 2019. The United Nations world water development report 2019: leaving no one behind. Paris, UNESCO. ⟨https://unesdoc.unesco.org/ark:/48223/pf0000367306⟩.

Wang, X., Müller, C., Elliot, J., Mueller, N.D., Ciais, P., Jägermeyr, J., Gerber, J., Dumas, P., Wang, C., Yang, H., Li, L., Deryng, D., Folberth, C., Liu, W., Makowski, D., Olin, S., Pugh, T.A.M., Reddy, A., Schmid, E., Jeong, S., Zhou, F., Piao, S., 2021. Global irrigation contribution to wheat and maize yield. Nat. Commun. 12 (1), 1235. https://doi.org/10.1038/s41467-021-21498-5.

Wei, J., Dirmeyer, P.A., Wisser, D., Bosilovich, M.G., Mocko, D.M., 2013. Where does the irrigation water go? An estimate of the contribution of irrigation to precipitation using MERRA. J. Hydrometeorol. 14 (1), 275–289. https://doi.org/10.1175/JHM-D-12-079.1.

Wongso, E., Nateghi, R., Zaitchik, B., Quiring, S., Kumar, R., 2020. A data-driven framework to characterize state-level water use in the United States. Water Resour. Res. 56 (9), e2019WR024894. https://doi.org/10.1029/2019WR024894.

Xu, T., Guo, Z., Xia, Y., Ferreira, V.G., Liu, S., Wang, K., Yao, Y., Zhang, X., Zhao, C., 2019. Evaluation of twelve evapotranspiration products from machine learning, remote sensing and land surface models over conterminous United States. J. Hydrol. 578, 124105. https://doi.org/10.1016/j.jhydrol.2019.124105.

Yang, Y., Jin, Z., Mueller, N.D., Driscoll, A.W., Hernandez, R.R., Grodsky, S.M., Sloat, L. L., Chester, M.V., Zhu, Y.-G., Lobell, D.B., 2023. Sustainable irrigation and climate feedbacks. Nat. Food 4 (8), 654–663. https://doi.org/10.1038/s43016-023-00821-x.

Yin, L., Feng, X., Fu, B., Chen, Y., Wang, X., Tao, F., 2020a. Irrigation water consumption of irrigated cropland and its dominant factor in China from 1982 to 2015. Adv. Water Resour. 143, 103661. https://doi.org/10.1016/j.advwatres.2020.103661.

Yin, Z., Wang, X.H., Ottlé, C., Zhou, F., Guimberteau, M., Polcher, J., Peng, S.S., Piao, S. L., Li, L., Bo, Y., Chen, X.L., Zhou, X.D., Kim, H., Ciais, P., 2020b. Improvement of the Irrigation Scheme in the ORCHIDEE land surface model and impacts of irrigation on regional water budgets over China. J. Adv. Model. Earth Syst. 12 (4), e2019MS001770. https://doi.org/10.1029/2019MS001770.

Zaussinger, F., Dorigo, W., Gruber, A., Tarpanelli, A., Filippucci, P., Brocca, L., 2019. Estimating irrigation water use over the contiguous United States by combining satellite and reanalysis soil moisture data. Hydrol. Earth Syst. Sci. 23 (2), 897–923. https://doi.org/10.5194/hess-23-897-2019.

Zaveri, E., B. Lobell, D., 2019. The role of irrigation in changing wheat yields and heat sensitivity in India. Nat. Commun. 10 (1), 4144. https://doi.org/10.1038/s41467-019-12183-9.

Zhang, Y., Kong, D., Gan, R., Chiew, F.H.S., McVicar, T.R., Zhang, Q., Yang, Y., 2019. Coupled estimation of 500 m and 8-day resolution global evapotranspiration and gross primary production in 2002–2017. Remote Sens. Environ. 222, 165–182. https://doi.org/10.1016/j.rse.2018.12.031.

Zhang, L., Li, X., Zheng, D., Zhang, K., Ma, Q., Zhao, Y., Ge, Y., 2021. Merging multiple satellite-based precipitation products and gauge observations using a novel double machine learning approach. J. Hydrol. 594, 125969. https://doi.org/10.1016/j.jhydrol.2021.125969.

Zhang, K., Li, X., Zheng, D., Zhang, L., Zhu, G., 2022a. Estimation of global irrigation water use by the integration of multiple satellite observations. Water Resour. Res. 58, e2021WR030031. https://doi.org/10.1029/2021WR030031.

Zhang, C., Long, D., 2021. Estimating spatially explicit irrigation water use based on remotely sensed evapotranspiration and modeled root zone soil moisture. Water Resour. Res. 57, e2021WR031382. https://doi.org/10.1029/2021WR031382.

Zhang, L., Ma, Q., Zhao, Y., Chen, H., Hu, Y., Ma, H., 2023. China's strictest water policy: reversing water use trends and alleviating water stress. J. Environ. Manag. 345, 118867. https://doi.org/10.1016/j.jenvman.2023.118867.

Zhang, L., Wang, W., Ma, Q., Hu, Y., Ma, H., Zhao, Y., 2024a. CCropLand30: high-resolution hybrid cropland maps of China created through the synergy of state-of-the-art remote sensing products and the latest national land survey. Comput. Electron. Agric. 218, 108672. https://doi.org/10.1016/j.compag.2024.108672.

Zhang, L., Xie, Y., Zhu, X., Ma, Q., Brocca, L., 2024b. CIrrMap250: annual maps of China's irrigated cropland from 2000 to 2020 developed through multisource data integration. Earth Syst. Sci. Data 16, 5207–5226. https://doi.org/10.5194/essd-2024-2.

Zhang, L., Zhang, K., Zhu, X., Chen, H., Wang, W., 2022b. Integrating remote sensing, irrigation suitability and statistical data for irrigated cropland mapping over mainland China. J. Hydrol. 613, 128413. https://doi.org/10.1016/j.jhydrol.2022.128413.

Zhang, L., Zheng, D., Zhang, K., Chen, H., Ge, Y., Li, X., 2022c. Divergent trends in irrigation-water withdrawal and consumption over mainland China. Environ. Res. Lett. 17 (9), 094001. https://doi.org/10.1088/1748-9326/ac8606.

Zheng, C., Jia, L., Zhao, T., 2023. A 21-year dataset (2000–2020) of gap-free global daily surface soil moisture at 1-km grid resolution. Sci. Data 10 (1), 139. https://doi.org/10.1038/s41597-023-01991-w.

Zhou, F., Bo, Y., Ciais, P., Dumas, P., Tang, Q., Wang, X., Liu, J., Zheng, C., Polcher, J., Yin, Z., Guimberteau, M., Peng, S., Ottle, C., Zhao, X., Zhao, J., Tan, Q., Chen, L., Shen, H., Yang, H., Piao, S., Wang, H., Wada, Y., 2020a. Deceleration of China's human water use and its key drivers. Proc. Natl. Acad. Sci. 117 (14), 7702. https://doi.org/10.1073/pnas.1909902117.

Zhou, T., Leung, L.R., Leng, G., Voisin, N., Li, H.-Y., Craig, A.P., Tesfa, T., Mao, Y., 2020b. Global irrigation characteristics and effects simulated by fully coupled land surface, river, and water management models in E3SM. J. Adv. Model. Earth Syst. 12 (10), e2020MS002069. https://doi.org/10.1029/2020MS002069.

Zhu, P., Burney, J., Chang, J., Jin, Z., Mueller, N.D., Xin, Q., Xu, J., Yu, L., Makowski, D., Ciais, P., 2022. Warming reduces global agricultural production by decreasing cropping frequency and yields. Nat. Clim. Change 12, 1016–1023. https://doi.org/10.1038/s41558-022-01492-5.

Zhu, P., Burney, J., 2022. Untangling irrigation effects on maize water and heat stress alleviation using satellite data. Hydrol. Earth Syst. Sci. 26 (3), 827–840. https://doi.org/10.5194/hess-26-827-2022.

Zhu, G., Zhang, K., Chen, H., Wang, Y., Su, Y., Zhang, Y., Ma, J., 2019. Development and evaluation of a simple hydrologically based model for terrestrial evapotranspiration simulations. J. Hydrol. 577, 123928. https://doi.org/10.1016/j.jhydrol.2019.123928.

Zohaib, M., Choi, M., 2020. Satellite-based global-scale irrigation water use and its contemporary trends. Sci. Total Environ. 714, 136719. https://doi.org/10.1016/j.scitotenv.2020.136719.